J. Fluid Mech. (2006), *vol.* 560, *pp.* 321–353.
doi:10.1017/S0022112006000620 Printed in the United Kingdom

Stability and instability of Taylor–Couette flows of a Bingham fluid

By M. P. LANDRY[1], I. A. FRIGAARD[1,2]† AND D. M. MARTINEZ[3]

[1]Department of Mathematics, University of British Columbia, 1984 Mathematics Road, Vancouver, BC, V6T 1Z2, Canada

[2]Department of Mechanical Engineering, University of British Columbia, 2054-6250 Applied Science Lane, Vancouver, BC, V6T 1Z4, Canada

[3]Department of Chemical and Biological Engineering, University of British Columbia, 2216 Main Mall, Vancouver, BC, V6T 1Z4, Canada

(Received 1 February 2005 and in revised form 3 January 2006)

We consider in detail the Taylor–Couette problem for a Bingham fluid, presenting a range of analytical and computational results. First, for co-rotating cylinders it is known that the critical inner cylinder Reynolds number $Re_{1,c}$, does not increase monotonically with the Bingham number B, over a range of small to moderate B. It is the only situation that we know of where a yield stress fluid flow is less stable that the corresponding Newtonian fluid flow. This effect was discovered independently by Landry (2003, MSc thesis) and Peng & Zhu (*J. Fluid Mech.* vol. 512, 2004, p. 21), but the mechanism has not been explained. Here we show that the decrease in critical Reynolds number is due to an increase (at small B) in the rate of strain of the basic flow, which amplifies the transfer of energy from the basic flow to the perturbation, via the inertial terms in the energy equation. At larger B, the yielded region contracts and the inertial energy transfer is bounded by the yield stress dissipation.

We next consider the effects of large B. For fixed radius and Reynolds number ratios, we show that for sufficiently large B all basic flows have an unyielded fluid layer attached to the outer wall. For these flows we show that there is a similarity mapping that maps both the basic solution and the linear stability problem onto the stability problem for an outer cylinder of radius equal to the yield surface radius. The Reynolds and Bingham numbers of the transformed problems are smaller than that of the original problem, as is the wavenumber k. As $B \to \infty$, the yield surface approaches the inner cylinder, defining a *narrow gap* limiting problem that differs from the classical narrow gap limit. Via the transformed problem we derive an energy estimate for stability: $Re_{1,c}k_c \sim B^{1.5}$ as $B \to \infty$, which compares well with our computed results for a stationary outer cylinder: $Re_{1,c} \sim B^{1.25}$ and $k_c \sim B^{0.375}$. We also show how $Re_{1,c} \sim B^{1.25}$ can be deduced from a simple order of magnitude analysis, for a stationary outer cylinder. Finally, we consider the second (classical) narrow gap limit in which the radius ratio η, approaches unity, for fixed B and Reynolds number ratio. We show that $Re_{1,c} \gtrsim (k^2[1 + O(B)] + \pi^2)/(1 - \eta)^{1/2}$ in this limit.

1. Introduction

The focus of this paper is the stability of Couette flow of a Bingham fluid. A Bingham fluid is the simplest model of a generalized Newtonian fluid that has a yield

† Author to whom correspondence should be addressed.

stress. This means that in regions where the shear stress lies below a critical limit the fluid behaves as an inelastic rigid solid. Such fluids were first considered by Bingham (1922), after whom the most commonly used model is named. Later, these fluids were studied more extensively by Oldroyd (1947), Prager (1954), Mossolov & Miasnikov (1965, 1966) and Duvaut & Lions (1976). Slightly more complex visco-plastic models are the Herschel–Bulkley and Casson models. These fluids occur both naturally and industrially, although often a visco-plastic model is an idealization of a more complex rheological (and/or thermophysical) behaviour. A range of different materials and a description of many of the known solutions to the Navier–Stokes equations is given by Bird, Dai & Yarusso (1983).

Suppose that we fill the gap between two coaxial cylinders with a yield stress fluid and slowly increase the torque on the inner cylinder. As the stress at the inner cylinder wall exceeds the yield stress of the fluid, the cylinders begin to rotate (see § 2.1). The fluid is yielded only in a thin layer next to the inner cylinder, while the outer part of the annulus remains undeformed and static. This is the basic Couette flow pattern for a yield stress fluid, see e.g. Bird *et al.* (1983). As the torque increases further, the yielded region grows outwards and eventually occupies the entire gap. Experience with Newtonian fluids, and knowledge of yield stress fluids in laboratory and industrial settings, suggests that this flow will lose its stability at a high enough rotation rate (or torque). A study of these flow instabilities is the subject of this paper.

Although our study is fundamental in nature, there are a number of practical applications in which shear-thinning and yield stress fluids flow between rotating cylinders. First, this is a key geometry for rotational rheometry and accurate rheological measurements using cylinders are obviously limited to shear rates below the Taylor-vortex limit. Secondly, rotational shear is used to thin axially flowing foodstuffs. For example, Fitt & Please (2001) consider a rotating heat exchanger between rotating cylinders. Thirdly, in paper making, fibres are fractionated in pressure screens in which the suspension flows axially in the annular space between an inner rotating cylinder and an outer porous wall. Lastly, in the drilling of oil wells the drill bit is attached to an inner cylinder, the drillstring, that rotates rapidly in the drilled hole. Here the onset of vortical structures is important because of two effects. First, in laminar wellbore hydraulic flows many authors have attempted to provide frictional pressure closures for different rheological models; e.g. Hansen *et al.* (1999), Bailey & Peden (2000), Diaz *et al.* (2004). In the case of slimhole drilling, where the annulus is relatively narrow, frictional pressure losses can account for 50–90 % of total pressure losses, and accurate prediction of the frictional pressure becomes very important for well planning. It has been observed that increasing rotation, at a constant axial flow rate, can both increase and decrease the frictional pressure losses (see McCann *et al.* 1993; Wang *et al.* 2000). This complex picture is partly attributable to the onset of vortical flow, which acts to shear-thin the drilling fluids. The second effect concerns the effects on cuttings transport (see e.g. Lockett, Richardson & Worraker 1993; Loureiro, Souza Mendes & Azevedo 2006). Attempts to study the onset of Taylor vortices in the oilfield context, for inelastic shear-thinning fluids, have been made by Lockett *et al.* (1992) and Coronado-Matutti, Souza Mendes & Carvalho (2004). In these papers, CFD codes are used to simulate the transient flow, and a numerical criterion is used to indicate transition, i.e. methodologically these are attempts to simulate a transition experiment, rather than direct studies of the hydrodynamic stability problem.

Taylor–Couette paradigm instabilities have been widely studied for Newtonian fluids. The reader may refer to Drazin & Reid (1981) and Drazin (2002) for an

overview, or to either one of the texts Koschmeider (1993) and Chossat & Iooss (1994) or papers by Di Prima & Swinney (1981), Andereck, Liu & Swinney (1986) and Tagg (1994) for detailed descriptions of the literature. There have also been a number of studies of the onset of Taylor vortices for non-Newtonian fluids. Principally these have concerned visco-elastic fluids, e.g. Larsen (1989, 1992), Muller, Larson & Shaqfeh (1989), Larson, Shaqfeh & Muller (1990), Joo & Shaqfeh (1992), Avgousti & Beris (1993), Muller *et al.* (1993), Joo & Shaqfeh (1994), Khayat (1995, 1997, 1999) Shaqfeh (1996), Al-Mubaiyedh, Sureshkumar & Khomami (2000), which are not of direct relevance here.

Yield stress fluids fall into the broad category of generalized Newtonian fluids. Certainly, Taylor vortices do occur in such fluids. This is evidenced by the numerical experiments of Lockett *et al.* (1992) and Coronado-Matutti, Souza Mendes & Carvalho (2004), by phenomenological evidence from applications such as oil well drilling (i.e. observed changes in frictional pressure), and also by direct experimental study. Nouar, Devienne & Lebouche (1987) and Naimi, Devienne & Lebouche (1990) have studied axial flow through an annulus with rotating inner cylinder, using CMC and Carbopol solutions, respectively. The former behaves as a power-law fluid and the latter has a yield stress, as well as shear-thinning behaviour. In both cases only axisymmetric Taylor vortices are reported, with their appearance retarded by the presence of an axial flow. Naimi *et al.* (1990) reports that the yield stress appears to stabilize the flow. The focus of the two studies is on heat transfer rather than hydrodynamic stability.

Considering specifically the study of Taylor–Couette hydrodynamic instabilities, for visco-plastic fluid flows, the most detailed studies are by Graebel (1964), Peng & Zhu (2004) and Landry (2003), (which we partly follow here). We should also mention a few shorter communications of numerical results that have appeared in various conference proceedings, Nsom & Mangel (2001), Coronado *et al.* (2002) and Lockett *et al.* (1993). Graebel (1964) was the first hydrodynamic linear stability study of a visco-plastic fluid flow, and it is unfortunate that this paper has remained hidden in conference proceedings for so long. The paper is largely analytical and considers axisymmetric linear disturbances. After correctly deriving the linearized stability equations and boundary conditions for the perturbed yield surface, Graebel proceeds to a narrow gap approximation of the classical type, which eventually allows analytical solutions using a truncated normal mode series, i.e. this is an extension of the classical methods for the Newtonian fluid, see e.g. Taylor (1923) and Chandrasekhar (1961). Graebel concludes that the Bingham fluid is more stable than the corresponding yield stress fluid.

This statement apparently contradicts results found independently by Landry (2003) and by Peng & Zhu (2004). Reduction of the critical Reynolds number with yield stress in wide gap co-rotating cylinders over a limited range of Bingham numbers was first reported by Landry (2003). The Bingham number denotes the ratio of yield stress to viscous stress, and hence we have the interesting observation that a positive yield stress may in fact be destabilizing. The focus of Peng & Zhu (2004) is a numerical study of instabilities of spiral Couette flow of a Bingham fluid and the majority of their paper concerns the spiral flow. In a short section of their paper, the Taylor–Couette case is also considered (i.e. where the inner cylinder does not slide). For co-rotating cylinders and at small radius ratios (meaning away from the narrow gap limit), Peng & Zhu also show that the critical Reynolds number first decreases and then increases with Hedström number, He (defined as $He = \hat{\tau}_y \hat{\rho} \hat{d}^2 / \hat{\mu}_p^2$), i.e. again the yield stress may destabilize.

In the context of the above results, a number of pieces of the puzzle are missing, and it is a goal of this paper to provide them. First of all, what is the physical/mathematical explanation for the decrease in critical Reynolds number? Secondly, how is it that Graebel (1964) predicts increasing stability with the yield stress (also in the case of co-rotating cylinders), whereas Landry (2003) and Peng & Zhu (2004) do not, i.e. is there a contradiction, or are these simply different results? Thirdly, it is apparent that as the yield stress increases (with all other parameters fixed), there will be a progressively thick unyielded layer of fluid attached to the outside wall. This results in a *narrow gap* of yielded fluid, in which the stability problem is posed. How does this narrow gap limit differ from that studied by Graebel (1964), or is it equivalent?

Apart from the above objectives, we comment that there has been practically no theoretical study of these flows for yield stress fluids. In the case of Newtonian fluids, such studies have led to simple heuristic rules and scaling laws that, although not always exact, often offer physical insight and practical utility, e.g. Rayleigh's criterion. As far as possible, we attempt to derive such results and explore other theoretical aspects of the stability problem.

An outline of our paper is as follows. We start by introducing the dimensionless equations and the basic flow. We present in § 2.1 a clear representation in the (Re_2, Re_1)-plane of the various transitions in the basic flow, between rigid rotations and flows with partial or no unyielded plug attached to the outer cylinder. We have found this representation helpful in developing our understanding. Section 3 develops the linear stability equations, and we focus solely on axisymmetric disturbances. A number of marginal stability results are presented in § 4. In § 4.1, we explain the origin of the non-monotonicity of the critical Reynolds number $Re_{1,c}$, with the Bingham number. Section 5 considers the case of rigid rotations, proving that the flows are linearly stable for all $B > 0$. We also develop an extended Rayleigh criterion. In § 6, we look at flows with an unyielded plug on the outer wall. As the Bingham number $B \to \infty$, these flows occupy the entire (Re_2, Re_1)-plane. We show that there is a similarity mapping of both the basic flow and stability problem onto an equivalent problem on an annulus with smaller outer cylinder. We also investigate the limit $B \to \infty$, producing asymptotic estimates for $Re_{1,c}$. We compare these against computed results for the case of stationary inner cylinder. In the final section, § 7, we consider the second narrow gap limit, namely that considered by Graebel (1964), in which $\eta \to 1$ at fixed B. The paper concludes with a short summary.

2. Problem formulation

We consider the flow between two infinitely long concentric cylinders with inner and outer radii, $\hat{R}_1$ and $\hat{R}_2$, that rotate independently with angular speeds $\hat{\Omega}_1$ (inner) and $\hat{\Omega}_2$ (outer). By convention, we take $\hat{\Omega}_1 > 0$. The scaled Navier-Stokes equations are:

$$\boldsymbol{u}_t + Re_1(\boldsymbol{u}\cdot\nabla)\boldsymbol{u} = -\nabla p + \nabla\cdot\boldsymbol{\tau}, \tag{2.1}$$

$$\nabla\cdot\boldsymbol{u} = 0, \tag{2.2}$$

where $\boldsymbol{u}$ is the velocity, p the pressure, $\boldsymbol{\tau}$ the deviatoric stress tensor, and Re_1 is the inner cylinder Reynolds number:

$$Re_1 = \frac{\hat{\rho}\hat{R}_1\hat{\Omega}_1\hat{d}}{\hat{\mu}_p}. \tag{2.3}$$

To scale these equations we have followed Chossat & Iooss (1994), with the aim of maintaining some compatibility of our notation with the various Newtonian results. Lengths have been scaled with the annular gap, $\hat{d} = \hat{R}_2 - \hat{R}_1$. Velocities are scaled with $\hat{\Omega}_1 \hat{R}_1$. The pressure and deviatoric stress are scaled with $\hat{\mu}_p \hat{R}_1 \hat{\Omega}_1 / \hat{d}$. Time is scaled with $\hat{\rho}\hat{d}^2/(\hat{\mu}_p)$. Here, $\hat{\rho}$ and $\hat{\mu}_p$ are the density and plastic viscosity, respectively.†

The constitutive laws describing the deformation of a Bingham fluid are:

$$\tau_{ij} = \left(1 + \frac{B}{\dot{\gamma}}\right) \dot{\gamma}_{ij} \iff \tau > B, \tag{2.4}$$

$$\dot{\gamma} = 0 \iff \tau \leqslant B, \tag{2.5}$$

where $\dot{\gamma}$ and τ are the second invariants of the rate of strain and deviatoric stress tensors, $\dot{\gamma} = \dot{\gamma}_{ij}$ and $\boldsymbol{\tau} = \tau_{ij}$, respectively. The Bingham number B above is defined as:

$$B = \frac{\hat{\tau}_y \hat{d}}{\hat{\mu}_p \hat{R}_1 \hat{\Omega}_1} \tag{2.6}$$

which represents a ratio of yield stress to viscous stress. Two further dimensionless groups will be used: the outer cylinder Reynolds number Re_2, and the radius ratio η:

$$Re_2 = \frac{\hat{\rho}\hat{R}_2\hat{\Omega}_2\hat{d}}{\hat{\mu}_p}, \qquad \eta = \frac{\hat{R}_1}{\hat{R}_2}. \tag{2.7}$$

To use He or B?

We follow Landry (2003) in representing yield stress effects via B, rather than $He = BRe_1$, as is done by Peng & Zhu (2004). In terms of the stability problem, both are evidently equivalent. Our choice of B is motivated by the basic Couette flows, which we show depend solely on B, η and Re_2/Re_1, and the simple representation of their change of type in the (Re_2, Re_1)-plane, which is the usual plane for plotting marginal stability results. This is explained in § 2.1.

Secondly, in using He, large values of He can correspond to modest values of B, (and hence relatively small qualitative changes in the basic flows), when exploring questions of stability since the Reynolds numbers are typically large. Thus, in Peng & Zhu (2004) we see relatively little perturbation from the Newtonian marginal stability results for large He, whereas later we explore the stability of a much fuller range of basic flows.

The interpretation of He, being the product BRe_1, is as the ratio of the product of inertial and yield stresses to the square of the viscous stresses, which is perhaps slightly obscure. The often cited advantage of He over B is that He depends only on fluid properties (incorrect as the geometry $\hat{d}$ also enters), whereas B depends on the process variables (i.e. velocity scale). In the end it is a matter of personal choice.

2.1. *Basic flow*

Below we consider the classical problem of linear stability, by perturbing a steady basic flow $\boldsymbol{U}$. It is well known that the configuration described admits a Couette velocity solution, $\boldsymbol{U} = (0, V(r), 0)$, in directions (r, θ, z) (see e.g. Bird *et al.* 1983). To

† The plastic viscosity represents the limiting viscosity of the fluid at infinite shear rate. In the absence of the yield stress it would correspond to the Newtonian viscosity. An incorrect interpretation often given in texts is that $\hat{\mu}_p$ represents the *constant viscosity* of the fluid when yielded. Such interpretations are only loosely valid for simple one-dimensional shear flows. In multi-dimensional flows these fluids have a non-constant nonlinear viscosity when yielded.

derive $V(r)$ we integrate the θ-momentum equation:

$$0 = \frac{1}{r^2}\frac{\partial}{\partial r}[r^2\tau_{r\theta}], \tag{2.8}$$

over $r \in [\eta/(1-\eta), 1/(1-\eta)]$ using the simplified constitutive laws for the shear flow:

$$\tau_{r\theta} = \left(1 + \frac{B}{|\dot{\gamma}_{r\theta}|}\right)\dot{\gamma}_{r\theta} \Longleftrightarrow |\tau_{r\theta}| > B, \tag{2.9}$$

$$|\dot{\gamma}_{r\theta}| = 0 \Longleftrightarrow |\tau_{r\theta}| \leqslant B, \tag{2.10}$$

$$\dot{\gamma}_{r\theta} = \frac{\mathrm{d}V}{\mathrm{d}r} - \frac{V}{r} \;=\; r\frac{\mathrm{d}}{\mathrm{d}r}\left[\frac{V}{r}\right]. \tag{2.11}$$

Equation (2.8) is effectively a second-order differential equation for $V(r)$ and consequently two boundary conditions are required. From the velocity scaling, these must be

$$V(\eta/(1-\eta)) = 1, \tag{2.12}$$

$$V(1/(1-\eta)) = \frac{Re_2}{Re_1}. \tag{2.13}$$

Thus, we see that $V(r)$ can be parameterized uniquely by B, η and Re_2/Re_1.

2.1.1. *Representation of $V(r)$ in the (Re_2, Re_1)-plane*

If we solve the system (2.8), (2.12) and (2.13), we find that the solutions are qualitatively of three types: (i) the cylinders may co-rotate at the same angular velocity, with the fluid fully unyielded in the annular gap; (ii) there may be a layer of unyielded fluid attached to the outer wall, together with a layer of yielded fluid at the inner wall; (iii) the fluid may be fully yielded throughout the annular gap.

Later we examine stability of the basic flow and present our results in the (Re_2, Re_1)-plane, as is conventional. It is convenient therefore to understand where the above three types of solution occur in the (Re_2, Re_1)-plane. It is therefore helpful to momentarily work with a stress boundary condition, rather than the velocity boundary conditions. We denote the inner wall shear stress as:

$$\tau_{r\theta}(\eta/(1-\eta)) = \tau_i. \tag{2.14}$$

Since $V(r)$ is parameterized uniquely by B, η and Re_1/Re_2, we can write that $\tau_i = \tau_i(B, \eta, Re_1/Re_2)$. To determine this relationship, we relax (2.12), find the solution corresponding to the two conditions (2.13) and (2.14), and then find τ_i such that (2.12) is satisfied. The advantage for this, admittedly roundabout route to $V(r)$, is a simple characterization of the basic flow types. From (2.8) and (2.14):

$$\tau_{r\theta} = \frac{\tau_i\eta^2}{r^2(1-\eta)^2}. \tag{2.15}$$

Therefore $\tau_{r\theta}$ does not change sign in the annulus and $|\tau_{r\theta}|$ decreases with r. Consequently, if there is an unyielded *plug* region in the annulus, it must be bounded inside by a yield surface, say at $r = R_y$, and must extend to the outside wall. The position R_y is defined where $|\tau_{r\theta}| = B$:

$$R_y = \frac{\eta}{1-\eta}\sqrt{\frac{|\tau_i|}{B}}. \tag{2.16}$$

The solution $V(r)$ is characterized in terms of τ_i as follows:

I.	Solid body rotation	$\dfrac{\lvert\tau_i\rvert}{B} \leqslant 1,$
II.	Partial plug	$1 < \dfrac{\lvert\tau_i\rvert}{B} \leqslant \left(\dfrac{1}{\eta}\right)^2,$
III.	No plug	$\left(\dfrac{1}{\eta}\right)^2 < \dfrac{\lvert\tau_i\rvert}{B}.$

Denoting $R_o = \min\{R_y, 1/(1-\eta)\}$, the velocity $V(r)$ is found to be:

$$V(r) = \begin{cases} \dfrac{Re_2(1-\eta)}{Re_1} r + \dfrac{\tau_i \eta^2 r}{2(1-\eta)^2}\left(\dfrac{1}{R_o^2} - \dfrac{1}{r^2}\right) + Br \ln\left(\dfrac{R_o}{r}\right) \operatorname{sgn}(\tau_i), & \eta/(1-\eta) \leqslant r \leqslant R_o, \\ \dfrac{Re_2(1-\eta)}{Re_1} r, & R_o \leqslant r \leqslant 1/(1-\eta). \end{cases} \tag{2.17}$$

For given B, η and Re_2/Re_1, it remains to find τ_i. By imposing (2.12), for cases II or III, we must solve:

$$1 = \frac{Re_2}{Re_1}\eta + \frac{\tau_i \eta}{2(1-\eta)}\left(\frac{\eta^2}{R_o^2(1-\eta)^2} - 1\right) + \frac{B\eta}{1-\eta} \ln\left(\frac{R_o(1-\eta)}{\eta}\right) \operatorname{sgn}(\tau_i),$$

which can be done either numerically (case II) or analytically (case III).

In the (Re_2, Re_1)-plane, for fixed (B, η), the velocity regimes of the basic flow are delineated by rays emanating from $(0, 0)$. For case I, imposing (2.12) implies that

$$\frac{Re_2}{Re_1} = \frac{1}{\eta}. \tag{2.18}$$

The boundaries between cases II and III are found when the stress at the outer wall reaches the yield stress, given by, i.e. $\tau_i = \pm B/\eta^2$. Denoting $f(\eta)$ by:

$$f(\eta) = \frac{1+\eta}{2\eta^2} - \frac{\ln(1/\eta)}{1-\eta},$$

we find that these boundaries are defined by

$$\frac{Re_2}{Re_1} = \frac{1}{\eta} \pm Bf(\eta). \tag{2.19}$$

An example is shown in figure 1(*a*). Observe that $f(\eta) > 0$. For small B, the partial plug regions are close to the rigid rotation line, $Re_2/Re_1 = 1/\eta$, but as B increases the two lines (2.19) fan out to incorporate an increasing proportion of the (Re_2, Re_1)-plane. Figure 1(*b*) illustrates the basic velocity $V(r)$ at a fixed $Re_1 = 200$, as Re_2 is increased through the different solution regimes. For $Re_2 = 0, 500$ there is a partial plug at the outer wall. This is indicated by a region within which $V(r) \propto r$, and is most visible when $Re_2 = 0$, since then $V(r) = 0$ in the plug. The same qualitative picture is found for other $\eta \in (0, 1)$ and $B > 0$.

3. Linear perturbation equations

We now consider the perturbation of our basic flow $(\boldsymbol{U}, P)$:

$$\boldsymbol{U} = (0, V(r), 0), \qquad P(r) = Re_1 \int^r \frac{V^2(\tilde{r})}{\tilde{r}}\, \mathrm{d}\tilde{r} + \text{ constant},$$

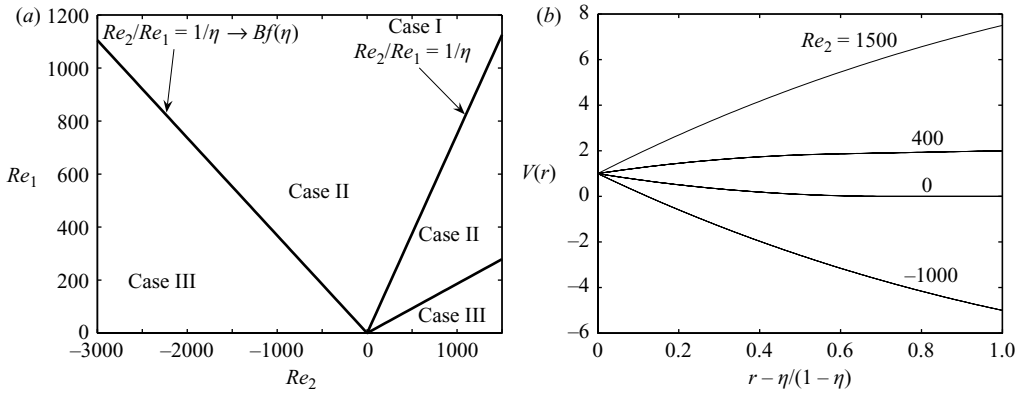

FIGURE 1. Examples of the basic flow at $\eta = 0.75$, $B = 10$: (*a*) flow regimes in the (Re_2, Re_1)-plane; (*b*) velocity profiles $V(r)$ at $Re_1 = 200$, $Re_2 = -2000, 0, 500, 1500$.

by a small disturbance

$$\epsilon \boldsymbol{u}' = (\epsilon u'(r,\theta,z,t), \epsilon v'(r,\theta,z,t), \epsilon w'(r,\theta,z,t)), \qquad \epsilon p'(r,\theta,z,t),$$

where $\epsilon \ll 1$. We straightforwardly derive the following linearized system of equations, valid in the yielded parts of the flow:

$$0 = \frac{\partial u'}{\partial r} + \frac{u'}{r} + \frac{1}{r}\frac{\partial v'}{\partial \theta} + \frac{\partial w'}{\partial z}, \tag{3.1}$$

$$\begin{aligned}\frac{\partial u'}{\partial t} = &-Re_1 \frac{V}{r}\left(\frac{\partial u'}{\partial \theta} - 2v'\right) - \frac{\partial p'}{\partial r} + \nabla^2 u' - \frac{2}{r^2}\frac{\partial v'}{\partial \theta} - \frac{u'}{r^2} \\ &+ B\left[\frac{1}{r}\frac{\partial}{\partial r}\left(\frac{r\dot\gamma_{rr}(\boldsymbol{u}')}{\dot\gamma(\boldsymbol{U})}\right) + \frac{1}{\dot\gamma(\boldsymbol{U})}\left(\frac{\partial}{\partial z}\dot\gamma_{rz}(\boldsymbol{u}') - \frac{\dot\gamma_{\theta\theta}(\boldsymbol{u}')}{r}\right)\right],\end{aligned} \tag{3.2}$$

$$\begin{aligned}\frac{\partial v'}{\partial t} = &-Re_1\left(u'\mathrm{D}_* V + \frac{V}{r}\frac{\partial v'}{\partial \theta}\right) - \frac{1}{r}\frac{\partial p'}{\partial \theta} + \nabla^2 v' + \frac{2}{r^2}\frac{\partial u'}{\partial \theta} - \frac{v'}{r^2} \\ &+ \frac{B}{\dot\gamma(\boldsymbol{U})}\left[\frac{1}{r}\frac{\partial}{\partial \theta}\dot\gamma_{\theta\theta}(\boldsymbol{u}') + \frac{\partial}{\partial z}\dot\gamma_{\theta z}(\boldsymbol{u}')\right],\end{aligned} \tag{3.3}$$

$$\begin{aligned}\frac{\partial w'}{\partial t} = &-Re_1 \frac{V}{r}\frac{\partial w'}{\partial \theta} - \frac{\partial p'}{\partial z} + \nabla^2 w' \\ &+ B\left[\frac{1}{r}\frac{\partial}{\partial r}\left(r\frac{\dot\gamma_{zr}(\boldsymbol{u}')}{\dot\gamma(\boldsymbol{U})}\right) + \frac{1}{\dot\gamma(\boldsymbol{U})}\left(\frac{1}{r}\frac{\partial}{\partial \theta}\dot\gamma_{z\theta}(\boldsymbol{u}') + \frac{\partial}{\partial z}\dot\gamma_{zz}(\boldsymbol{u}')\right)\right],\end{aligned} \tag{3.4}$$

where

$$\mathrm{D} = \frac{\mathrm{d}}{\mathrm{d}r}, \qquad \mathrm{D}_* = \frac{\mathrm{d}}{\mathrm{d}r} + \frac{1}{r},$$

and $\dot\gamma = \dot\gamma(\boldsymbol{U})$. The latter is evaluated from the basic flow and the constitutive laws, which give:

$$\dot\gamma(\boldsymbol{U}) = |\dot\gamma_{r\theta}| = \frac{|\tau_i|\eta^2}{(1-\eta)^2 r^2} - B. \tag{3.5}$$

3.1. *Boundary conditions*

If we set $B = 0$ in (3.1)–(3.4), we recover the Newtonian stability problem, for which appropriate boundary conditions are:

$$\boldsymbol{u}' = 0 \quad \text{at} \quad r = \eta/(1-\eta), \tag{3.6}$$

$$\boldsymbol{u}' = 0 \quad \text{at} \quad r = 1/(1-\eta). \tag{3.7}$$

If $B > 0$, we must consider the type of basic flow. For a case III basic solution, the flow is yielded everywhere and the boundary conditions are (3.6) and (3.7).

For a case II basic solution, we have a partial plug in the annulus, for $r \in [R_y, 1/(1-\eta)]$. The perturbation $(\epsilon \boldsymbol{u}', \epsilon p)$ is augmented with a linear perturbation of the yield surface, i.e. $R_y \to R_y + \epsilon r_y(\theta, z, t)$. Implicit here is the assumption of a linear perturbation of the deviatoric stress. The linearization leading to (3.1)–(3.4) is then carried out only in the perturbed yielded region, $r \in [\eta/(1-\eta), R_y + \epsilon r_y]$, which is linearized onto the yielded region of the basic flow $r \in [\eta/(1-\eta), R_y]$. The boundary condition (3.6) is evidently applicable at the inner cylinder. At the outer cylinder, (3.7) is also satisfied. However, the linear stability problem is now posed on $r \in [\eta/(1-\eta), R_y]$.

At the yield surface, both velocity and stress (i.e. traction) vectors are continuous. We linearize these conditions both with respect to the perturbations $(\epsilon \boldsymbol{u}', \epsilon p')$ and onto R_y. The method is explained in more detail in Frigaard, Howison & Sobey (1994). To transfer the conditions at the outer cylinder to those at $r = R_y$, we observe that for $r \in [R_y + \epsilon r_y, 1/(1-\eta)]$, we have that $\dot{\gamma}(\boldsymbol{U} + \epsilon \boldsymbol{u}') = 0$. Thus, $\dot{\gamma}(\boldsymbol{u}') = 0$ and we readily find that:

$$\boldsymbol{u}' = 0 \quad \text{at} \quad r = R_y. \tag{3.8}$$

Whereas (3.8) is the correct boundary condition at $r = R_y$, a number of additional conditions also arise from continuity of stress at the perturbed yield surface:

$$\dot{\gamma}_{rr}(\boldsymbol{u}') = \dot{\gamma}_{\theta\theta}(\boldsymbol{u}') = \dot{\gamma}_{zz}(\boldsymbol{u}') = 0 \quad \text{at} \quad r = R_y, \tag{3.9}$$

$$\dot{\gamma}_{rz}(\boldsymbol{u}') = \dot{\gamma}_{z\theta}(\boldsymbol{u}') = 0 \quad \text{at} \quad r = R_y, \tag{3.10}$$

$$\dot{\gamma}_{r\theta}(\boldsymbol{u}') = \frac{2 r_y B \operatorname{sgn}(\tau_i)}{R_y} \quad \text{at} \quad r = R_y. \tag{3.11}$$

These conditions are not strictly boundary conditions. Instead, (3.9) and (3.10) are compatibility conditions. Observe that each $\dot{\gamma}_{ij}(\boldsymbol{u}')$ in (3.9) and (3.10) also appears in the Bingham terms in (3.2)–(3.4), divided by $\dot{\gamma}(\boldsymbol{U})$. Conditions (3.9) and (3.10) are therefore necessary conditions for the linear stability equations to be well-defined as $r \to R_y^-$ (as we expect from a physical standpoint). We observe that $\dot{\gamma}_{r\theta}(\boldsymbol{u}')$ does not appear among the Bingham terms in (3.2)–(3.4). Condition (3.11) is therefore not required for compatibility, but instead defines the perturbation of the yield surface, R_y, from the perturbed solution. Note that the yield surface is not a material surface or *interface*, so there is no kinematic condition.

Lastly, we note that for a case I basic flow, there is no yielded region and no linear stability problem. Apart from the critical case where $|\tau_i| = B$ (and then only at $r = \eta/(1-\eta)$), the shear stress is everywhere below the yield stress by a finite amount. We have assumed only a linear perturbation of the deviatoric stress everywhere, and therefore the finite plug that fills the annulus cannot be perturbed by an infinitesimal perturbation.

3.2. *Axisymmetric disturbances*

From here onwards we consider axisymmetric disturbances only. For Newtonian fluids these are the least stable modes except for strongly counter-rotating cylinders. For generalized Newtonian fluids, only axisymmetric vortices were reported in the experimental studies of Nouar *et al.* (1987) and Naimi *et al.* (1990). Also in some preliminary experiments we have carried out at UBC, we have only seen axisymmetric vortices. However, in all these experiments the outer cylinder is fixed, so spiral flows are not expected anyway.

Mathematically, we have no rigorous justification of axisymmetry for all B and all (Re_2, Re_1). If we derive a linear energy equation, inclusion of the azimuthal derivatives contributes directly to the destabilizing inertial term only in terms of the phase speed of a linear disturbance and not the growth rate. In the viscous term, the azimuthal derivatives simply increase the dissipation rate. However, analogous observations hold true for all generalized Newtonian fluids. In the limit $B \to 0$, following the methods in Duvaut & Lions (1976), it is often possible to prove continuity of the Bingham fluid solution in this Newtonian limit. This being the case, we would expect that azimuthal instabilities are the least stable, at low B, for co-rotating and weakly counter-rotating cylinders.

We proceed in the usual fashion, assuming a normal mode expansion of the perturbation, of the form:

$$(u', v', w', p') \sim (u(r), v(r), w(r), p(r))\, \mathrm{e}^{\lambda t + \mathrm{i}kz}, \tag{3.12}$$

and $r_y = h\, \mathrm{e}^{\lambda t + \mathrm{i}kz}$ when we have a case II basic flow. Substituting into (3.1)–(3.4):

$$\mathrm{D}_* u + \mathrm{i}kw = 0, \tag{3.13}$$

$$(\mathrm{D}\mathrm{D}_* - k^2 - \lambda)u = -2Re_1 \left(\frac{V}{r}\right) v + \mathrm{D}p - B\phi_r, \tag{3.14}$$

$$(\mathrm{D}\mathrm{D}_* - k^2 - \lambda)v = Re_1(\mathrm{D}_* V)u + k^2 B \frac{v}{\dot\gamma(\boldsymbol{U})}, \tag{3.15}$$

$$(\mathrm{D}_*\mathrm{D} - k^2 - \lambda)w = \mathrm{i}kp - B\phi_z, \tag{3.16}$$

where

$$\phi_r = \frac{1}{r}\mathrm{D}\left(\frac{2r\mathrm{D}u}{\dot\gamma(\boldsymbol{U})}\right) + \frac{1}{\dot\gamma(\boldsymbol{U})}\left(\mathrm{i}k\mathrm{D}w - k^2 u - \frac{2u}{r^2}\right), \tag{3.17}$$

$$\phi_z = \frac{1}{r}\mathrm{D}\left(\frac{r(\mathrm{i}ku + \mathrm{D}w)}{\dot\gamma(\boldsymbol{U})}\right) - \frac{2k^2 w}{\dot\gamma(\boldsymbol{U})}. \tag{3.18}$$

Using (3.13) to eliminate w and then (3.16) to eliminate p results in a fourth-order eigenvalue problem for u, coupled to a second-order eigenvalue problem for v. Writing $\boldsymbol{x} = (u, v)$, our eigenvalue system becomes

$$\mathscr{A}\boldsymbol{x} = \lambda \mathscr{B}\boldsymbol{x}, \tag{3.19}$$

where

$$\mathscr{A} = \mathscr{A}_V + Re_1 \mathscr{A}_I + B\mathscr{A}_Y, \tag{3.20}$$

respectively denoting the viscous, inertial and yield stress parts of $\mathscr{A}$. These operators

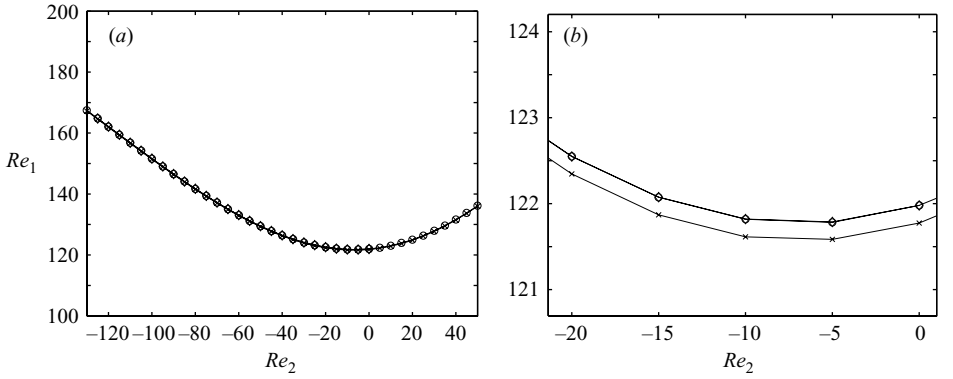

FIGURE 2. Marginal stability curve for a Newtonian fluid: $\eta = 0.883$. Comparison $\times$, of finite difference method results, $N = 50$, $\circ$, Chebychev expansion results, $N = 50$, and $\diamond$, those computed by R. Tagg.

are defined by

$$\mathscr{A}_V = \begin{pmatrix} (\mathrm{D}\mathrm{D}_* - k^2)^2 & 0 \\ 0 & k^2 - \mathrm{D}\mathrm{D}_* \end{pmatrix}, \qquad \mathscr{A}_I = \begin{pmatrix} 0 & -2k^2\left(\dfrac{V}{r}\right) \\ \mathrm{D}_* V & 0 \end{pmatrix},$$

$$\mathscr{A}_Y = \begin{pmatrix} L_Y & 0 \\ 0 & \dfrac{k^2}{\dot{\gamma}(\boldsymbol{U})} \end{pmatrix}, \qquad \mathscr{B} = \begin{pmatrix} \mathrm{D}\mathrm{D}_* - k^2 & 0 \\ 0 & -1 \end{pmatrix},$$

where

$$L_Y u = -k^2\phi_r - \mathrm{i}k\mathrm{D}\phi_z = (\mathrm{D}\mathrm{D}_* - k^2)\left[\frac{\mathrm{D}\mathrm{D}_* - k^2}{\dot{\gamma}(\boldsymbol{U})}\right]u. \tag{3.21}$$

The boundary conditions are:

$$u = \mathrm{D}u = v = 0 \quad \text{at} \quad r = \eta/(1-\eta), \tag{3.22}$$

$$u = \mathrm{D}u = v = 0 \quad \text{at} \quad r = R_o, \tag{3.23}$$

see our previous discussion. For case II basic flows, the normal mode forms of the compatibility conditions (3.9)–(3.10) are also satisfied, and (3.11) defines the modal amplitude of the yield surface perturbation.

Note that the block structure of the Newtonian operator $\mathscr{A}_V + \mathscr{A}_I$ is preserved when the yield stress terms are added, and that L_Y is real. It should also be noted that fourth-order derivatives appear in the operator L_Y.

3.3. *Computational method and validation*

We have solved the system (3.19) numerically, using both finite-difference methods and a Chebyshev discretization (essentially as described in Schmid & Henningson 2001). For fixed (Re_1, Re_2, k), we solve for the eigenvalues and eigenfunctions of (3.19), and take the eigenvalue with maximal real part, $\lambda_{R,max}(k)$. At each (Re_1, Re_2) pair, an inner iteration then computes the wavenumber k_{max}, for which $\lambda_{R,max}$ is largest. For the outer iteration, in general we fix Re_2 and increase Re_1 until $\lambda_{R,max} = 0$ is found, using a bisection method.

The results are quite similar using both discretization methods and acceptable convergence is found for $N \approx 30$ (here N denotes the number of Chebyshev polynomials in our approximation). In figure 2 and table 1, we show a comparison

$Re_2 =$	0	−5	−10	−25	−50	−100
FD	121.7749	121.5845	121.6138	123.0273	129.2676	151.3940
CP	121.9805	121.7822	121.8188	123.2324	129.4653	151.6064
Tagg	121.9791	121.7868	121.8205	123.2306	129.4683	151.6083

TABLE 1. Values of critical Re_1 computed via the finite-difference method (FD), and Chebychev expansion (CP), compared with results from R. Tagg. Parameters: $\eta = 0.883$, $N = 50$.

against numerical values supplied by R. Tagg for the corresponding Newtonian fluid problem, $B = 0$. It can be seen that the results are very close. For the remaining results in the paper, we have used the Chebyshev expansion with $N = 50$ points (unless otherwise stated). The matrices involved in the Chebyshev expansion are smaller than the finite-difference method and hence computation is quicker.

4. Marginal stability

Sample marginal stability curves for increasing values of B are shown in figure 3, at $\eta = 0.883$. We also plot the domain boundaries that separate type I, II and III base solutions. We observe that for this radius ratio, the critical Re_1 increases monotonically with B. All curves lie above the rigid rotation line $Re_1 = \eta Re_2$. Linear instability is predicted both when the annulus is fully yielded (case III) and when there exists an unyielded plug on the outer wall (case II). The transition is smooth along the marginal stability curve, between case III and case II base solutions. We might expect there to be some form of discontinuity in the marginal curve as it crosses the boundary between case III and case II, since the case II stability problem has the additional boundary constraints (3.9) and (3.10) imposed at the yield surface (which is the outer boundary). As explained earlier, these additional constraints arise only because $\mathscr{A}_Y$ becomes singular at the yield surface, and simply act to ensure that $\mathscr{A}_Y \boldsymbol{x}$ is non-singular.

Figure 4 shows marginal stability curves for a wider range of parameters. For counter-rotating cylinders the results are qualitatively similar to those for the case $\eta = 0.833$. However, as the gap is widened we see an interesting effect for co-rotating cylinders. Over a range of B, at fixed Re_2, it would appear that increasing B decreases the critical Reynolds number. For large enough B, the critical Reynolds number increases. This effect is more pronounced at smaller η (radius ratio).

The features most evident in figures 3 and 4 are as follows. (i) For counter-rotating cylinders, the stability is enhanced by increasing B. (ii) The minimal critical values of Re_1 are found for slightly counter-rotating cylinders. (iii) For co-rotating cylinders, different behaviours are observed for small and large η. In the narrow gap case, $\eta \approx 1$, it appears that increasing B is purely stabilizing. For wider gaps the stability is non-monotone.

In figure 5, we show some examples of the spectra and variation of $\lambda_{R,max}(k)$, at two different points on the marginal stability curve for $\eta = 0.75$, $B = 5$; see figure 4(c). For those values that we have computed, the eigenvalue with the largest real part is real, although there are also a few complex eigenvalues.

4.1. *Non-monotonicity*

Probably the most interesting feature of the results is the non-monotonicity of the critical Reynolds number Re_1, for co-rotating cylinders as B is increased. This

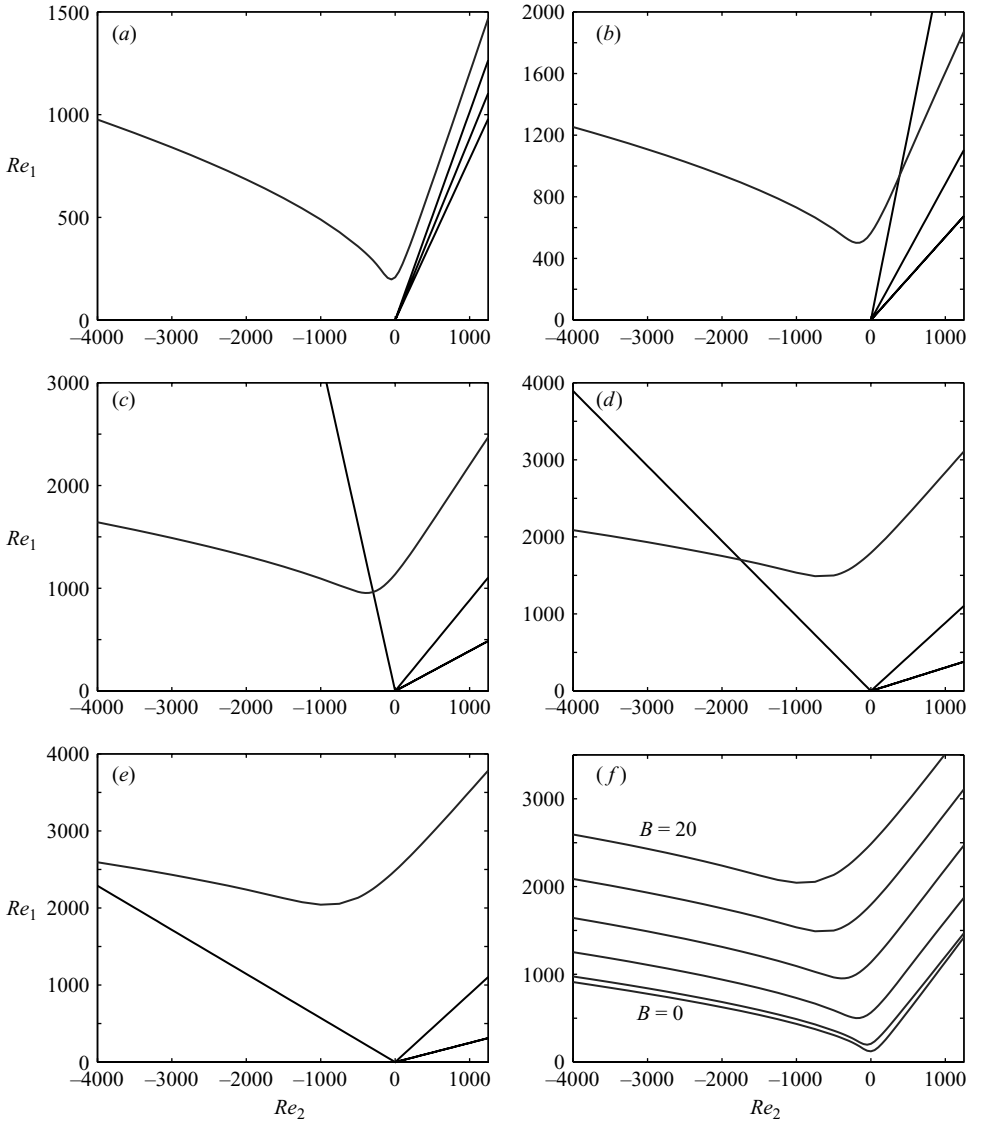

FIGURE 3. Marginal stability curves and basic flow types for various B: $\eta = 0.883$, $N = 50$. (*a*) $B = 1$; (*b*) $B = 5$; (*c*) $B = 10$; (*d*) $B = 15$; (*e*) $B = 20$; (*f*) All curves overlayed, plus Newtonian $B = 0$.

surprising behaviour is most observable in a wide gap cylinder, (small η) and is the only visco-plastic flow that we know of, for which increasing B apparently destabilizes the flow. Figure 6 plots the variation in $Re_{1,crit}$ with B, for $\eta = 0.5, 0.6$. We can see that the effect is very significant for $Re_2 > 100$, and occurs over moderate ranges of B, e.g. $0 < B \lesssim 1$. Although this effect has been reported in Peng & Zhu (2004), it has not been explained, i.e. physically how is it that an increase in B can lead to a less stable flow? First, we note from figure 6 that there is no apparent relation with the change in the type of base solution as B increases.

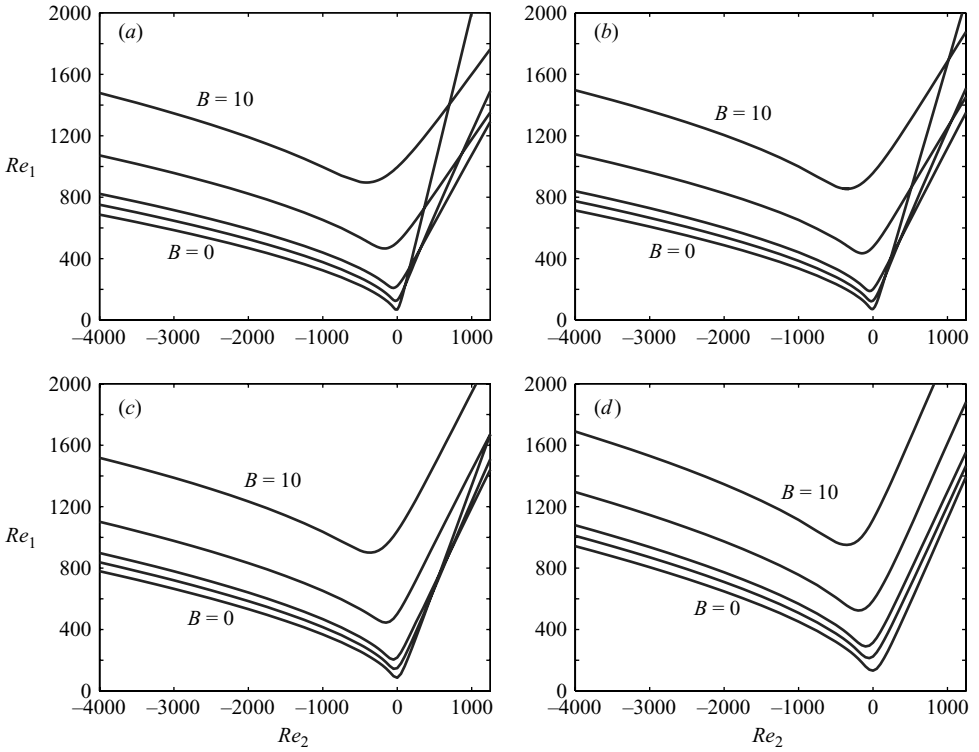

FIGURE 4. Marginal stability curves and basic flow types for $B = 0, 1, 2, 5, 10$: $N = 50$. (*a*) $\eta = 0.5$; (*b*) $\eta = 0.6$; (*c*) $\eta = 0.75$; (*d*) $\eta = 0.9$.

On multiplying (3.14)–(3.16) by r times the complex conjugate, $\bar{\boldsymbol{u}} = (\bar{u}, \bar{v}, \bar{w})$, then integrating from $R_1 = \eta/(1-\eta)$ to R_o, we derive the linear energy equality:

$$\lambda \|\boldsymbol{u}\|^2 = Re_1 J_I - J_V - B J_Y, \tag{4.1}$$

where J_I, J_V and J_Y, denote inertial, viscous and yield stress contributions to the kinetic energy growth of the perturbations. These are defined by:

$$\|\boldsymbol{u}\|^2 = \int_{R_1}^{R_o} r(|u|^2 + |v|^2 + |w|^2)\,\mathrm{d}r, \tag{4.2}$$

$$J_I = \int_{R_1}^{R_o} \left(2V v\bar{u} - r\left(\mathrm{D}V + \frac{V}{r}\right)\bar{v}u\right)\mathrm{d}r, \tag{4.3}$$

$$J_V = \int_{R_1}^{R_o} \left(r|\mathrm{D}\boldsymbol{u}|^2 + k^2 r|\boldsymbol{u}|^2 + \frac{|u|^2 + |v|^2}{r}\right)\mathrm{d}r, \tag{4.4}$$

$$J_Y = \int_{R_1}^{R_o} \frac{1}{\dot{\gamma}}\left(2\left(r|\mathrm{D}u|^2 + \frac{|u|^2}{r}\right) + rk^2(|v|^2 + 2|w|^2) + r|ku - \mathrm{i}\mathrm{D}w|^2\right)\mathrm{d}r. \tag{4.5}$$

Note that both J_V and J_Y are real and positive, representing dissipation. Only the real part of J_I, say $J_{I,R}$, contributes to λ_R, and can cause instability. In the case where we are above the rigid rotation line ($\tau_i < 0$), and if the critical eigenvalues and eigenfunctions are real (which we have found to be the case for co-rotating cylinders),

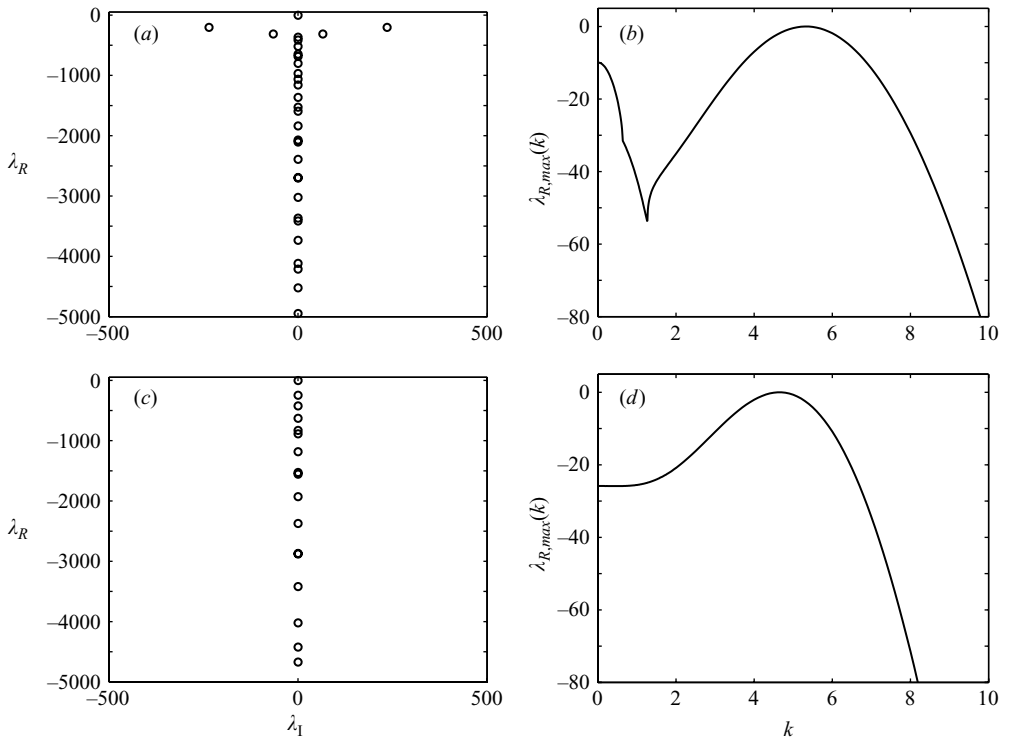

FIGURE 5. Example spectra and maximal eigenvalues at different points on the marginal stability curve for $B = 5$, $\eta = 0.75$, $N = 50$. (a, b) $Re_1 = 529.6533$, $Re_2 = -500$, case I basic solution: spectrum at $k_{max} = 5.3292$ and variation of $\lambda_{R,max}(k)$; (c, d) $Re_1 = 938.3018$, $Re_2 = 500$, case II basic solution: spectrum at $k_{max} = 4.6529$ and variation of $\lambda_{R,max}(k)$.

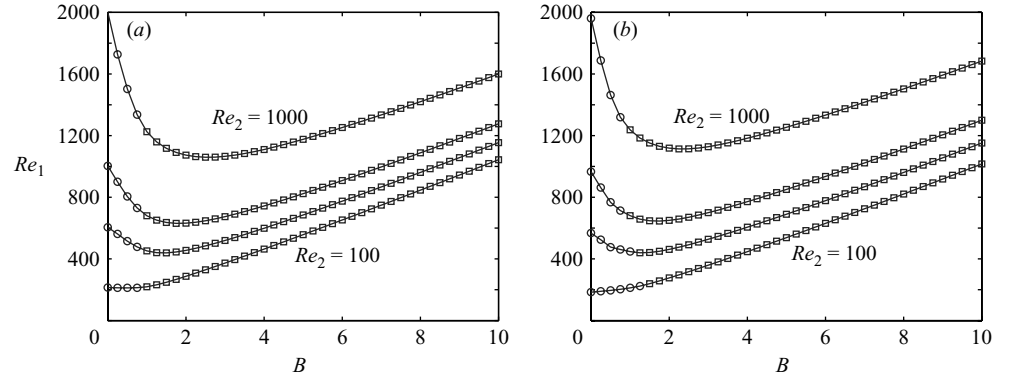

FIGURE 6. Marginal stability curves in co-rotating cylinders for $Re_2 = 100, 300, 500, 1000$; $N = 50$: (a) $\eta = 0.5$; (b) $\eta = 0.6$. □, case 2, partially yielded base solution; ○, fully yielded base solution.

we have

$$J_I = J_{R,I} = \int_{R_1}^{R_o} -r\left(\mathrm{D}V - \frac{V}{r}\right)(v_R u_R + v_I u_I)\,\mathrm{d}r = \int_{R_1}^{R_o} r\dot{\gamma}(r) v_R u_R\,\mathrm{d}r. \qquad (4.6)$$

By definition, marginal stability comprises a balance between the dissipative terms $J_V + BJ_Y$ and the inertial term $Re_1 J_I$. The fact that the critical Re_1 decreases with B

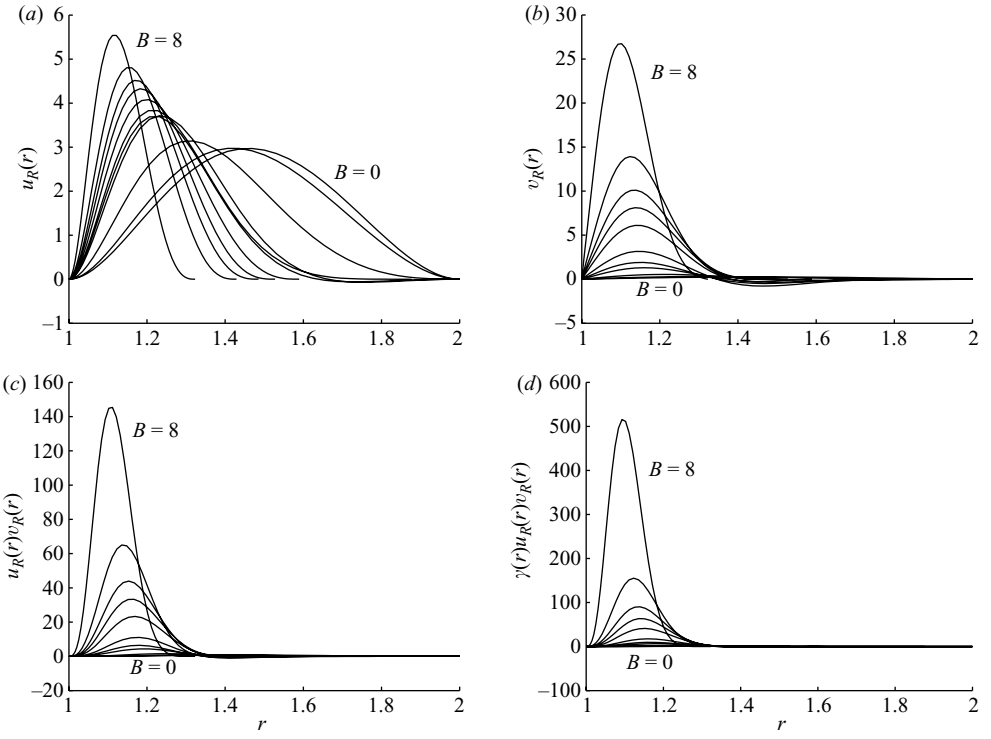

FIGURE 7. Critical eigenfunctions and the integrand of $J_{I,R}$ for varying marginally stable $Re_{1,c}(B)$; $\eta = 0.5$, $Re_2 = 500$, $B = 0, 0.01, 0.05, 0.25, 0.5, 1, 2, 2.5, 3, 4, 8$. (*a*) $u_R(r)$; (*b*) $v_R(r)$; (*c*) $u_R(r)v_R(r)$; (*d*) $u_R(r)v_R(r)\dot{\gamma}(r)$, the integrand of $J_{I,R}$.

over some range implies precisely that

$$Re_{1,c} = \frac{J_V + BJ_Y}{J_{I,R}}, \tag{4.7}$$

decreases with B over some range, (when the functionals are evaluated with the marginal eigenfunctions). The functionals J_V, $J_{I,R}$ and J_Y are characterized as follows:

(i) J_V depends only on the eigenfunctions, whereas both $J_{I,R}$ and J_Y depend upon the eigenfunctions and the rate of strain of the basic flow, $\dot{\gamma}(r)$.

(ii) $J_{I,R}$ increases with $\dot{\gamma}(r)$ whereas J_Y decreases with $\dot{\gamma}(r)$.

(iii) J_V and J_Y contain quadratic products of the eigenfunctions and their first derivatives, whereas $J_{I,R}$ contains only the product uv.

Obviously, increase of $Re_{1,c}(B)$ in (4.7) has to be due to changes with B, in either $\dot{\gamma}(r)$ or the eigenfunctions. Since the problem is linear, we may scale one of the eigenfunctions, and here we choose to normalize the eigenfunctions so that the L^2 norm of $u_R(r)$ is equal to 1. If now we have an increase in the size of $|v_R|$ with B, we see that J_V and J_Y will increase quadratically, whereas $J_{I,R}$ increases only linearly. Conversely, if $|v_R|$ decreases with B, the normalized $u_R(r)$ dominates. Consequently, it appears that changes in the eigenfunctions with B cannot be responsible for the increase of $Re_{1,c}(B)$, and the effect has to be due to the rate of strain.

Let us examine the eigenfunctions, and how they combine in the inertial integral $J_{I,R}$. We follow the marginal stability curve for $Re_2 = 500$, $\eta = 0.5$ and increasing B. The critical values of Re_1, as B increases, are shown in figure 6(*a*). In figure 7(*a*, *b*)

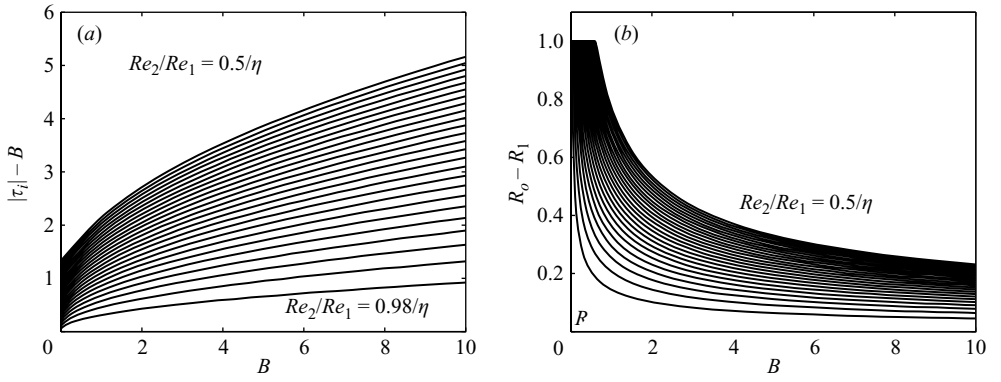

FIGURE 8. (*a*) $\dot{\gamma}_{max} = |\tau_i| - B$, for $Re_2/Re_1 = 0.5/\eta, 0.52/\eta, \ldots, 0.98/\eta$, all at $\eta = 0.5$; (*b*) $R_o - R_1$, for $Re_2/Re_1 = 0.5/\eta, 0.52/\eta, \ldots, 0.98/\eta$, all at $\eta = 0.5$.

we plot the (real) eigenfunctions $u_R(r)$ and $v_R(r)$, as we traverse this curve increasing B. In figure 7(*c*, *d*) we plot the product $u_R(r)v_R(r)$, and the integrand of $J_{I,R}$, i.e. $u_R(r)v_R(r)\dot{\gamma}(r)$.

The main features are as follows. First, only for small values, $0 \leqslant B \lesssim 1$, do we have a type III basic solution: fully yielded fluid filling the annular gap. As B increases, we see that the critical eigenfunctions are non-zero only in a progressively small yielded layer of width $(R_o - R_1)$. By virtue of the normalization we expect that, $u_R(r) \sim O([R_o - R_1]^{-1/2})$, which increases relatively slowly with B as the yielded gap closes. These effects appear well represented in figure 7(*a*). A more significant effect is seen in figure 7(*b*), where the azimuthal velocity v_R appears to increase rapidly with B (i.e. much more so than $u_R(r)$). The product $u_R(r)v_R(r)$ therefore also grows with B. However, as discussed, this in itself is not necessarily destabilizing. Examining carefully figure 7(*d*), we see that multiplication by $\dot{\gamma}(r)$ in fact amplifies the differences between the curves in figure 7(*c*). This implies that $\dot{\gamma}(r)$ increases with B in the yielded part of the annulus. Note that $\dot{\gamma}(r)$ multiplies the inertial terms in $J_{I,R}$, but divides the dissipative terms in J_Y. Therefore, this is the source of destabilization.

To confirm this, figure 8(*a*) plots the maximal value of $\dot{\gamma}(r)$, (always found at the inner cylinder), against B for a range of ratios, Re_2/Re_1, that lie above the rigid rotation line, $Re_2/Re_1 = 1/\eta$, i.e. covering the domain where the marginal curves lie. We see that $\dot{\gamma}_{max}$ generally increases with B. For a range of B close to zero, we have $\dot{\gamma}_{max} \sim B^{\nu}$. As B increases, for $|\tau_i| \sim B$ we can derive asymptotically that $\nu \sim 1/2$, whereas further from the rigid rotation line it appears that the growth exponent $\nu \sim 1$, for small B. At larger B, the rate of increase is certainly less than linear. We therefore assume the estimate $0.5 < \nu < 1$, and consider the ratios $J_V/J_{I,R}$ and $J_Y/J_{I,R}$ for small B. Supposing that $\dot{\gamma} \sim \dot{\gamma}_{max}$, and that the width of the yielded part of the annulus remains constant (a case III solution), then (4.7) implies that

$$Re_{1,c} \sim B^{-\nu} + B^{1-2\nu}, \tag{4.8}$$

which decreases. This effect may be modulated by changes in the eigenfunctions with B, as we have discussed.

As B increases, the width of yielded fluid decreases. The dissipation terms contain derivatives of the eigenfunctions, and so we may estimate

$$\frac{J_V}{J_{I,R}} \sim \frac{1}{\dot{\gamma}[R_o - R_1]^2}, \frac{J_Y}{J_{I,R}} \sim \frac{1}{\dot{\gamma}^2[R_o - R_1]^2},$$

with $\dot{\gamma}$ some representative scale for the rate of strain. Figure 8(b) plots ($R_o - R_1$) against B, over a range of Re_2/Re_1 that lies above the rigid rotation line, $Re_2/Re_1 = 1/\eta$. For a small range of B close to zero, $R_o - R_1 = 1$, and then ($R_o - R_1$) decreases with B. The rate of decrease at large B can be estimated as $(R_o - R_1) \sim B^{-1/2}$. Assuming this, we may estimate $Re_{1,c}$ for large B:

$$Re_{1,c} \sim B^{1-\nu} + B^{2-2\nu}, \tag{4.9}$$

for $0.5 < \nu < 1$. Hence $Re_{1,c}(B)$ increases for large enough B, and the non-monotone behaviour in $Re_{1,c}$ is explained. Probably the range of B over which $Re_{1,c}(B)$ decreases is approximately that over which $R_o - R_1 = 1$, although we have not tested this hypothesis. Physically, over a small range of B, transfer of energy from the basic flow to the perturbation is enhanced by an increase in the rate of strain of the basic flow. As B increases further, the yielded fluid domain decays to zero, eliminating the possibility for energy transfer.

5. Case I solutions – stability of co-rotating cylinders

For all the computed marginal stability results, we have found instability only above the rigid rotation line, $Re_2/Re_1 = 1/\eta$, which marks where case I basic solutions are found. For a rigid rotation, the linearization cannot be meaningfully carried out (apart from in the critical case where the inner cylinder wall stress exactly matches the yield stress). Although on physical grounds we must expect that rigid rotations are stable to linear perturbations, we should like to provide a more rigorous proof. We consider the real part of the linear energy equality (4.1):

$$\lambda_R \|\boldsymbol{u}\|^2 = Re_1 J_{I,R} - J_V - B J_Y. \tag{5.1}$$

Applying the incompressibility condition, the Cauchy–Schwarz inequality and the Poincaré inequality, Landry (2003) shows that conservative bounds for $J_{I,R}$, J_V and J_Y are, respectively:

$$J_{I,R} \leqslant \frac{\dot{\gamma}_{max}}{2}\left(\frac{R_o}{R_1}\right)^{1/2}(R_o - R_1)(k^2\|v\|^2 + \|w\|^2), \tag{5.2}$$

$$J_V \geqslant \min\left\{1, \frac{R_1}{R_o}\frac{\pi^2}{(R_o - R_1)^2}\right\}(k^2\|v\|^2 + \|w\|^2), \tag{5.3}$$

$$J_Y \geqslant \frac{1}{\dot{\gamma}_{max}}\min\left\{1, \frac{R_1}{R_o}\frac{\pi^2}{(R_o - R_1)^2}\right\}(k^2\|v\|^2 + \|w\|^2). \tag{5.4}$$

Combining the bounds (5.2), (5.3) and (5.4), it follows that

$$\frac{\lambda_R \|\boldsymbol{u}\|^2}{k^2\|v\|^2 + \|w\|^2} \leqslant \left[\frac{Re_1\dot{\gamma}_{max}}{2}\left(\frac{R_o}{R_1}\right)^{1/2}(R_o - R_1) - \left(1 + \frac{B}{\dot{\gamma}_{max}}\right)C(R_o, R_1)\right],$$

where

$$C(R_o, R_1) = \min\left\{1, \frac{R_1}{R_o}\frac{\pi^2}{(R_o - R_1)^2}\right\}.$$

Evidently, as the rigid rotation line is approached, $R_o \to R_1$, thus $C(R_o, R_1) = 1$, and we have that $\lambda_R < 0$ provided that:

$$Re_1 < \frac{2B}{(R_o - R_1)\dot{\gamma}_{max}^2}\left(\frac{R_1}{R_o}\right)^{1/2} \to \infty. \tag{5.5}$$

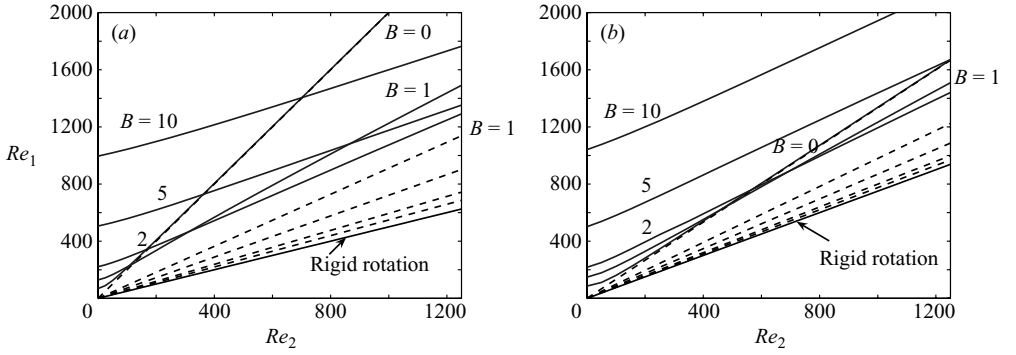

FIGURE 9. Comparison of the extended Rayleigh criterion (5.6) (dashed lines) with computed marginal stability results (solid lines) and the rigid rotation line, at $B = 0, 1, 2, 5, 10$: (*a*) $\eta = 0.5$; (*b*) $\eta = 0.75$.

The various inequalities leading to (5.5) are of course not sharp, and as a stability bound, (5.5) compares poorly to the computed results. However, (5.5) demonstrates rigorously that the rigid rotation line, $Re_1 = \eta Re_2$, is linearly stable for all configurations. In fact, the bound (5.5) defines an envelope, below and above $Re_1 = \eta Re_2$. Finally, we comment also that the above approach is directly applicable to non-axisymmetric perturbations. The additional inertial terms contribute only to λ_I, whereas both J_V and J_Y are increased.

5.1. *An extended Rayleigh criterion*

Close examination of the marginal stability curves that we have computed for $B > 0$, indicates that the marginal stability curves lie considerably above the rigid rotation line $Re_1 = \eta Re_2$. For Newtonian fluids, not only is $Re_1 < \eta Re_2$ stable to linear axisymmetric disturbances, but also $Re_1 < Re_2/\eta$. The latter is Rayleigh's criterion, which was initially advanced heuristically for viscous flows by Rayleigh (1916), but was later proved to be valid for linear axisymmetric flows by Synge (1938). In fact, Rayleigh's criterion is known to provide a good estimate of the marginal stability curve for Newtonian fluids, when the cylinders are co-rotating and when both Reynolds numbers are large. It is natural to ask whether the same is true for a yield stress fluid.

Rayleigh's argument is based on the conservation of the circulation $\hat{r}\hat{V}(\hat{r})$ in a rotating inviscid flow with no azimuthal pressure gradient. For a steady rotation, the consequence of this is that $\hat{p} + \hat{\rho}\hat{V}^2/2$ does not vary with $\hat{r}$. It is then argued that such flows will be stable only if exchange of the radial position of two rings of fluid does not result in a net release of kinetic energy. In the case of a Bingham fluid, the same heuristic reasoning may be applied to the basic flow. The following Rayleigh criterion is straightforwardly developed for co-rotating cylinders, with $V(r) > 0$, above the rigid rotation line.

$$\frac{Re_2}{Re_1} \geqslant \frac{B}{2(1-\eta)}\left[\ln\left(\frac{R_o}{R_1}\right)^2 + \frac{|\tau_i|}{B}\left(\frac{R_1}{R_o}\right)^2 - 1\right] \Longrightarrow \text{Stable}. \tag{5.6}$$

The physical interpretation is the same as for the Newtonian fluid.

In figure 9, we plot the bound from the extended Rayleigh criterion (5.6), against our previously computed marginal stability results for various B at $\eta = 0.5$ and $\eta = 0.75$. At large Re_k, we see that the Newtonian curves converge rapidly to the Rayleigh criterion. The marginal curves for $B > 0$ do not converge to the extended

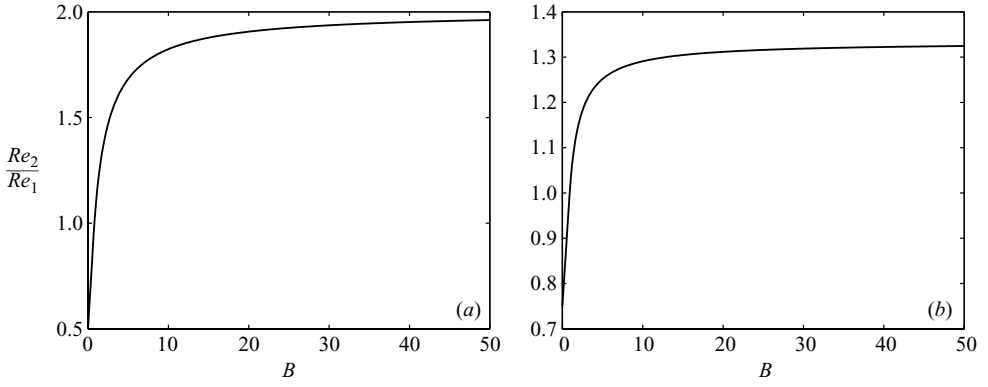

FIGURE 10. Variation with B of Re_2/Re_1 computed from the extended Rayleigh criterion (5.6): (*a*) $\eta = 0.5$; (*b*) $\eta = 0.75$.

Rayleigh criterion (5.6). However, it appears that the slope of the marginal stability curves at large Re_k is close to that of the extended Rayleigh criterion. There appears to be a constant offset that increases with B. The second observation is that for each η, as B increases from zero, the critical slope Re_2/Re_1, predicted from (5.6), appears to increase from the Newtonian value, η, towards the rigid rotation value, $1/\eta$, as $B \to \infty$. We plot this ratio in figure 10.

These results hint at a straightforward extension of the Rayleigh criterion for visco-plastic fluids. We may argue that the rotational flows will be unstable only if an exchange of the radial position of two rings of fluid acts to release enough kinetic energy to overcome the yield stress, i.e. we simply impose a threshold dependence on B. As an intuitive physical interpretation this is perhaps useful, but since the marginal stability curves are computed easily anyway, the practical and predictive value of such an heuristic criterion is debatable.

Lastly, we have not attempted to prove that (5.6) provides a lower bound on stability for linear axisymmetric disturbances, although this appears to be true for all our results. The method of Synge (1938) relies on the simple format of $V(r)$ for the Newtonian flow, i.e. $V(r) = ar + b/r$. This allows formulation of two linearized energy equations that can be subtracted to eliminate the inertial terms containing products of u and v, and thence to an energy bound. Unfortunately the same method applied here does not seem straightforward, since the velocity profile is more complex.

6. Case II solutions and the yielded narrow gap, as $B \to \infty$

It is natural to ask what the marginal stability behaviour is at large B. Solving the eigenvalue problem for large B, we find increasing values of $Re_{1,c}$, but the computations become progressively less well-conditioned. For large B, note that the lines

$$\frac{Re_2}{Re_1} = \frac{1}{\eta} \pm Bf(\eta),$$

fan progressively outwards to encompass the entire (Re_2, Re_1)-half-plane. Therefore, for any fixed rotation rates and geometry, as the yield stress increases, eventually the basic solution is a case II solution. It appears sensible to study these solutions more closely.

By focusing solely on those case II solutions for which $\tau_i < -B$ (i.e. dimensional rotation rates for which $\hat{\Omega}_1 > \hat{\Omega}_2$ which is where instability is found), we may derive the following expansions at large B:

$$\frac{|\tau_i|}{B} \sim 1 + \frac{A_0}{B^{1/2}} + \frac{A_0^2}{3B} + \frac{11A_0^3}{72B^{3/2}} + O(B^{-2}), \tag{6.1}$$

$$\frac{R_o(1-\eta)}{\eta} \sim 1 + \frac{A_0}{2B^{1/2}} + \frac{A_0^2}{24B} + \frac{A_0^3}{18B^{3/2}} + O(B^{-2}), \tag{6.2}$$

where

$$A_0 = 2(1-\eta)^{1/2}\left[\frac{1}{\eta} - \frac{Re_2}{Re_1}\right]^{1/2}. \tag{6.3}$$

Note that A_0 is fixed on each ray, $Re_2/Re_1 =$ constant, and, as $B \to \infty$, the annular gap of yielded fluid, $R_o - \eta/(1-\eta) \sim B^{-1/2}$. Since the linear stability problem is posed on the yielded layer only, it appears that at large B we should consider a narrow gap problem on the thin yielded layer. In § 7, we will consider a second narrow gap limit, namely $\eta \to 1$ for fixed B, which is essentially the classical Taylor limit and leads to a case I solution. However, for the study of the effects of large B, this second narrow gap problem is of little relevance.

6.1. *A similarity mapping for the case II stability problem*

Before studying the effects of large B, we note that there exists a similarity mapping for case II solutions. Observing the identical form of $V(r)$ in the yielded region for case II and case III solutions leads us to consider whether there exists a mapping from every case II solution onto a case III solution. We see in § 6.1.1 that this is indeed the case. This leads us to question whether there is also a mapping that maps each case II stability problem to a corresponding case III stability problem, which we answer affirmatively in § 6.1.2.

6.1.1. *Case II basic solutions*

We consider only case II solutions for which $\tau_i < -B$, (a similar mapping may be applied for $\tau_i > B$). Mapping of the basic solutions consists of a simple re-scaling of the length, i.e. we define

$$r^* = \frac{r}{R_o - \eta/(1-\eta)},$$

and simply match the coefficients in (2.17). The velocity profile becomes:

$$V(r^*) = \frac{Re_2^*(1-\eta^*)}{Re_1^*} r^* + \frac{\tau_i^*(\eta^*)^2 r^*}{2}\left(1 - \frac{1}{[r^*(1-\eta^*)]^2}\right) - B^* r^* \ln\left(\frac{1}{r^*(1-\eta^*)}\right),$$

$$\frac{\eta^*}{1-\eta^*} \leqslant r^* \leqslant \frac{1}{1-\eta^*}, \tag{6.4}$$

from which we deduce the following mappings:

$$\eta^* = \frac{\eta}{R_o(1-\eta)}, \tag{6.5}$$

$$\frac{Re_2^*}{Re_1^*} = \frac{Re_2}{Re_1} R_o(1-\eta), \tag{6.6}$$

$$B^* = B[R_o - \eta/(1-\eta)], \tag{6.7}$$

$$\tau_i^* = \tau_i[R_o - \eta/(1-\eta)]. \tag{6.8}$$

The inner wall stress τ_i^* is now determined from the condition that R_o is a yield surface for the non-transformed solution, i.e.

$$\tau_i^* = \tau_i[R_o - \eta/(1-\eta)] = -B\left(\frac{R_o^2(1-\eta)}{\eta^2}\right)[R_o - \eta/(1-\eta)] = -\frac{B^*}{(\eta^*)^2}.$$

Therefore, we can write

$$V(r^*) = \frac{Re_2^*(1-\eta^*)}{Re_1^*}r^* - \frac{B^*r^*}{2}\left[1 - \frac{1}{[r^*(1-\eta^*)]^2} + \ln\left(\frac{1}{[r^*(1-\eta^*)]^2}\right)\right].$$

Since $V(r^*)=1$ at $r^* = \eta^*/(1-\eta^*)$, we have:

$$\frac{1}{\eta^*} = \frac{Re_2^*}{Re_1^*} - \frac{B^*}{2(1-\eta^*)}\left[1 - \frac{1}{(\eta^*)^2} + \ln\left(\frac{1}{(\eta^*)^2}\right)\right] = \frac{Re_2^*}{Re_1^*} + B^* f(\eta^*),$$

i.e. for the transformed solution, described in terms of $(Re_2^*/Re_1^*, \eta^*, B^*)$, we lie on the boundary between case II and case III solutions. We may also observe that $\eta^* \geqslant \eta$, $|Re_2^*|/Re_1^* \leqslant |Re_2|/Re_1$ and $B^* \leqslant B$. We state the following proposition.

Proposition 1. *For every case II solution with $\tau_i < -B$, the velocity field $V(r)$ is equivalent to a case III velocity field $V(r^*)$, where $V(r^*)$ is the velocity field between a pair of cylinders with a narrower annular gap. For the equivalent velocity field $V(r^*)$, the Bingham number and the absolute value of the Reynolds number ratio are reduced. The transformed case III solution is that which attains the yield stress exactly at the outer cylinder, i.e. it is a borderline case II–III solution.*

Finally, we may eliminate Re_2^*/Re_1^* from the basic solution, since we are concerned only with the borderline case II–III solutions:

$$V(r^*) = \frac{r^*(1-\eta^*)}{\eta^*} - \frac{B^*r^*}{2(\eta^*)^2}\left[1 - \frac{(\eta^*)^2}{[r^*(1-\eta^*)]^2} + (\eta^*)^2\ln\left(\frac{(\eta^*)^2}{[r^*(1-\eta^*)]^2}\right)\right], \quad (6.9)$$

6.1.2. *Case II stability problems*

To show that every case II stability problem maps to a marginal case II–III stability problem, we re-scale all radial distances and the wavenumbers. The eigenvalue problems are then identical, with the new definitions:

$$k^* = k[R_o - \eta/(1-\eta)], \quad (6.10)$$

$$\lambda^* = [R_o - \eta/(1-\eta)]^2\lambda, \quad (6.11)$$

$$Re_1^* = [R_o - \eta/(1-\eta)]Re_1, \quad (6.12)$$

$$Re_2^* = Re_2R_o(1-\eta)[R_o - \eta/(1-\eta)]. \quad (6.13)$$

This result is only possible because the boundary conditions at the yield surface are identical and because the compatibility conditions are homogeneous and must be satisfied on the boundary case II–III basic solutions. Clearly, the above mapping preserves the stability characteristics of the eigenvalue problem since λ is simply scaled.

Proposition 2. *Not only does each case II basic solution map to a borderline case II–III basic solution, but also the linear stability is preserved in this mapping. The parameter space of the linear stability problem for case II solutions is therefore reduced by one dimension. It suffices to solve the linear stability problem and find the marginal point*

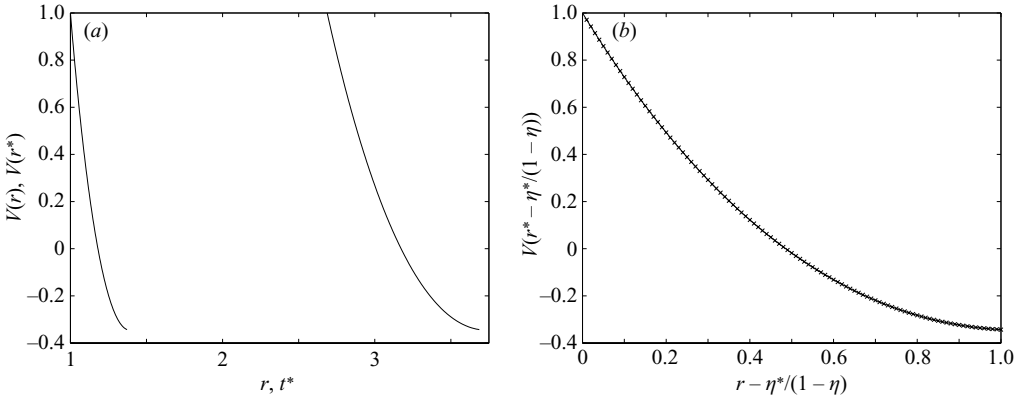

FIGURE 11. $B = 10$, $\eta = 0.5$, $Re_1 = 200$, $Re_1 = -100$. (*a*) $V(r)$ and $V(r^*)$; (*b*) $V((r - R_1)/(R_o - R_1))$ and $V(r^* - \eta^*/(1 - \eta^*))$.

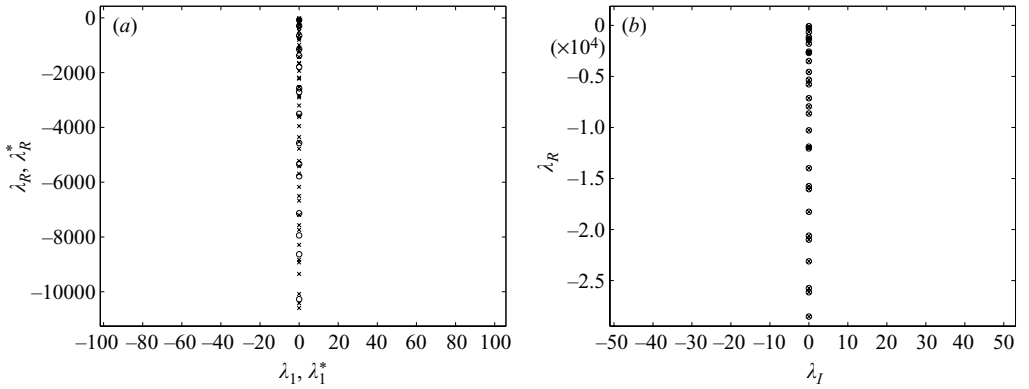

FIGURE 12. $B = 10$, $\eta = 0.5$, $Re_1 = 200$, $Re_1 = -100$. (*a*) Spectra λ and λ^*; (*b*) λ and λ^* superimposed.

along the line

$$\frac{Re_2^*}{Re_1^*} = \frac{1}{\eta^*} - B^* f(\eta^*), \tag{6.14}$$

for each (η^*, B^*). *Since every marginal case II solution maps onto one such point, this set describes all the marginal stability curves for all* (Re_1, Re_2, η, B) *that admit case II solutions. The critical Reynolds numbers of the transformed problems, are smaller:* $Re_{k,c}^* < Re_{k,c}$, $k = 1, 2$. *The growth rate of an unstable disturbance is smaller for the transformed problem and the wavenumbers of a disturbance are scaled with the width of the yielded fluid region,* $R_o - \eta/(1 - \eta)$.

6.1.3. *Examples*

We verify the validity of the above transformation in figures 11 and 12, which show the mapping for both the basic flow velocity profile and for the spectrum of an eigenvalue problem, respectively. In figures 11(*b*) and 12(*b*), the velocity profiles and spectra of the different mappings are superimposed upon one another.

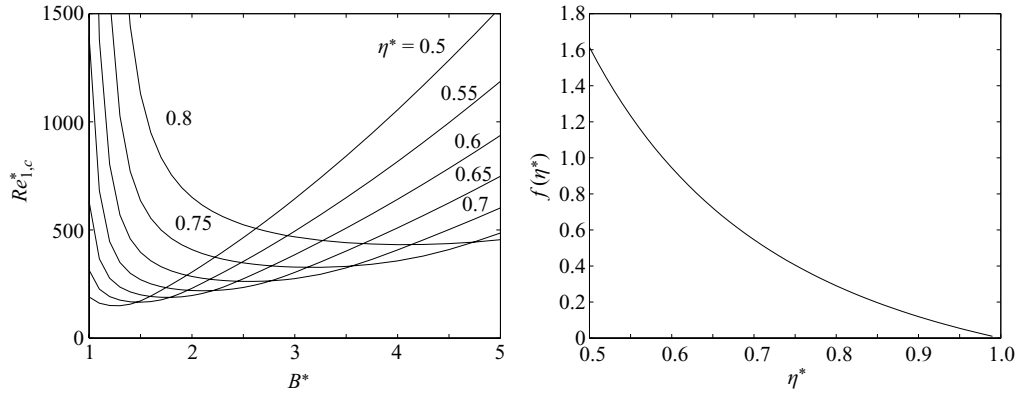

FIGURE 13. (*a*) Marginal stability curves $Re^*_{1,c}(\eta^*, B^*)$; (*b*) the function (η^*).

6.2. *Marginal stability:* $Re^*_{1,c}(\eta^*, B^*)$

The similarity mapping of §§ 6.1.1 and 6.1.2 provides an efficient method of computing the marginal stability values. For each (η^*, B^*) we fix the ratio Re^*_2/Re^*_1 according to (6.14), which defines $V(r^*)$ and then solve the eigenvalue problem in the starred variables. This defines $Re^*_{1,c}(\eta^*, B^*)$, which is the critical value of Re^*_1, computed along the ray $Re^*_2/Re^*_1 =$ fixed, defined by (6.14). Some examples are shown in figure 13.

We can see that $Re^*_{1,c}(\eta^*, B^*)$ increases both for large and small B^*. At small B^*, the line separating case II and III basic solutions approaches the rigid rotation line, and hence $Re^*_{1,c}(\eta^*, B^*)$ grows. For large B^*, the line separating case II and III basic solutions approaches the Re^*_2-axis, and at the same time we can seen that for counter-rotating cylinders the marginal stability curves are nested above one another as B increases. Since the Reynolds numbers are reduced in the transformed problem, the computation is slightly better conditioned.

6.3. *The narrow gap limit of large B*

As discussed, when $B \to \infty$ any basic solution at fixed $(Re_2/Re_1, \eta)$ becomes a case II solution. Equation (6.2) gives the asymptotic rate of decay of $R_o \to \eta/(1-\eta)$, as $B \to \infty$. Furthermore, under the similarity transform discussed in § 6.1, for each case II basic solution the stability problem is equivalent to that of a borderline case II–III basic solution. We may therefore investigate the limit $B \to \infty$ via its effect on the transformed problems.

For large B we see that $\eta^* \to 1$, $B^* \to \infty$ and $k^* \to 0$, according to:

$$1 - \eta^* \sim \frac{A_0}{2B^{1/2}} - \frac{5A_0^2}{24B} + O\left(B^{-3/2}\right), \tag{6.15}$$

$$B^* \sim B^{1/2}\frac{R_1 A_0}{2}\left[1 + \frac{A_0}{12B^{1/2}} + \frac{A_0^2}{9B} + O\left(B^{-3/2}\right)\right], \tag{6.16}$$

$$k^* \sim k\frac{R_1 A_0}{2B^{1/2}}\left[1 + \frac{A_0}{12B^{1/2}} + \frac{A_0^2}{9B} + O\left(B^{-3/2}\right)\right], \tag{6.17}$$

where $R_1 = \eta/(1-\eta)$. We write

$$r^* = \frac{\eta^*}{1-\eta^*} + \xi,$$

substitute into (6.9) and derive the leading-order expansion for the basic velocity as $B \to \infty$:

$$V(r^*) \sim 1 - \frac{R_1 A_0^2}{4}[2\xi - \xi^2] + O\left(B^{-1/2}\right). \tag{6.18}$$

Similarly, we derive:

$$\frac{\mathrm{d}V(r^*)}{\mathrm{d}r^*} \sim -\frac{R_1 A_0^2}{2}(1-\xi) + O\left(B^{-1/2}\right), \tag{6.19}$$

$$\left|\frac{\mathrm{d}V(r^*)}{\mathrm{d}r^*} - \frac{V(r^*)}{r^*}\right| \sim \frac{R_1 A_0^2}{2}(1-\xi) + O\left(B^{-1/2}\right), \tag{6.20}$$

where in (6.20) the higher-order terms also vanish as $\xi \to 1$.

We now transform the eigensystem (3.19) to the ξ variable and take the limit $B \to \infty$. To retain coupling through the inertial terms, we define:

$$\tilde{u} = u, \qquad \tilde{v}\frac{B}{k}\left[\frac{2}{R_1 A_0^2}\right]^{1/2} = v, \tag{6.21}$$

$$\tilde{\lambda} = \lambda^*, \qquad \tilde{R}e_1 = \frac{Re_1^* k}{B}\left[\frac{R_1 A_0^2}{2}\right]^{3/2}. \tag{6.22}$$

Our leading-order eigensystem is:

$$\mathrm{D}_\xi^2\left[\frac{\mathrm{D}_\xi^2 \tilde{u}}{1-\xi}\right] - \tilde{R}e_1\left(1 - \frac{R_1 A_0^2}{4}[2\xi - \xi^2]\right)\tilde{v} = 0, \tag{6.23}$$

$$\mathrm{D}_\xi^2 \tilde{v} + \tilde{R}e_1(1-\xi)\tilde{u} = \tilde{\lambda}\tilde{v}, \tag{6.24}$$

where $\mathrm{D}_\xi = \mathrm{d}/\mathrm{d}\xi$. Boundary conditions are:

$$\tilde{u} = \mathrm{D}_\xi \tilde{u} = \tilde{v} = 0 \qquad \text{at} \quad \xi = 0, \tag{6.25}$$

$$\tilde{u} = \mathrm{D}_\xi \tilde{u} = \tilde{v} = 0 \qquad \text{at} \quad \xi = 1, \tag{6.26}$$

plus the various compatibility conditions at $\xi = 1$, to remove the singularity.

This eigensystem is degenerate, and requires some form of regularization to solve numerically. However, we may proceed to bound $\tilde{\lambda}_R$, using an energy method. Denoting $\alpha = R_1 A_0^2/4$, we multiply (6.23) by $\bar{u}$, (6.24) by $\alpha\bar{v}$, integrate over $[0, 1]$ and retain only the real part, to give:

$$\alpha\tilde{\lambda}_R \int_0^1 |\tilde{v}|^2 \mathrm{d}\xi = -\alpha \int_0^1 |\mathrm{D}\tilde{v}|^2 \mathrm{d}\xi - \int_0^1 \frac{|\mathrm{D}^2\tilde{u}|^2}{1-\xi}\,\mathrm{d}\xi + \tilde{R}e_1 \int_0^1 \left(1 + \alpha[1 - 3\xi + \xi^2]\right)(\tilde{v}_R\tilde{u}_R + \tilde{v}_I\tilde{u}_I)\,\mathrm{d}\xi. \tag{6.27}$$

Using the Poincaré and Cauchy-Schwarz inequalities, we bound as follows:

$$\begin{aligned}\alpha\tilde{\lambda}_R||\tilde{v}||^2 &\leqslant -\pi^2(\alpha||\tilde{v}||^2 + \pi^2||\tilde{u}||^2) + \frac{\tilde{R}e_1(1+\alpha)}{2}\left(\frac{\sqrt{\alpha}}{\pi}||\tilde{v}||^2 + \frac{\pi}{\sqrt{\alpha}}||\tilde{u}||^2\right) \\ &\leqslant -\left(\pi^2 - \frac{\tilde{R}e_1(1+\alpha)}{2\pi\sqrt{\alpha}}\right)\left(||\tilde{v}||^2 + \frac{\pi^2}{\alpha}||\tilde{u}||^2\right),\end{aligned} \tag{6.28}$$

and therefore $\tilde{\lambda}_R \leqslant 0$, provided that:

$$\tilde{R}e_1 \leqslant \frac{2\pi^3\sqrt{\alpha}}{1+\alpha}. \tag{6.29}$$

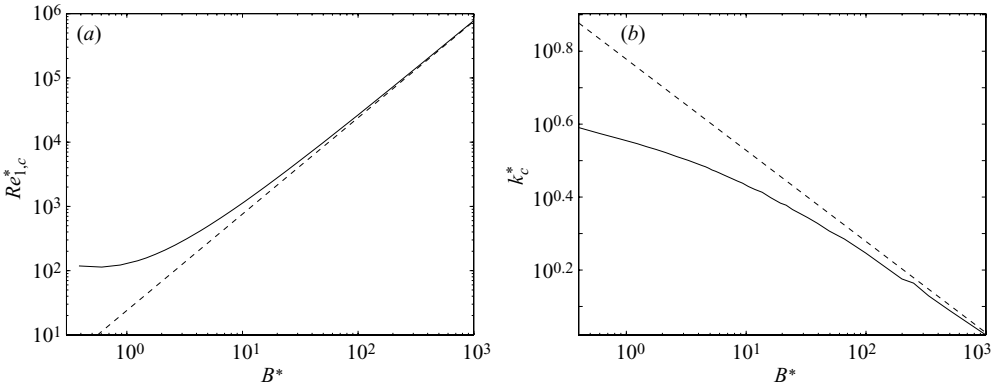

FIGURE 14. Stationary outer cylinder: (*a*) marginal stability curves $Re^*_{1,c}$ *vs.* B^*, dashed line is $Re^*_1 = 24(B^*)^{1.5}$; (*b*) wavenumbers k^*_c at critical $Re^*_{1,c}$, plotted against B^*, dashed line is $k^*_c = 6(B^*)^{-0.25}$.

In terms of the starred and unstarred variables, as $B \to \infty$, this approximate stability limit is:

$$Re^*_1 k^* \leqslant \frac{2\pi^3 B^*}{\alpha(1+\alpha)}, \tag{6.30}$$

$$Re_1 k \leqslant \frac{2\pi^3 A_0 B^{3/2}}{\alpha^2(1+\alpha)}. \tag{6.31}$$

Below, we shall consider how good these estimates are.

6.4. *Stationary outer cylinder:* $Re_2 = Re^*_2 = 0$

It is not sensible to compute marginal stability results for all values of Re^*_2/Re^*_1. The case when the outer cylinder is fixed, $Re_2 = Re^*_2 = 0$, is, however, of particular practical interest. For example, rotational shear is often used to thin industrial fluids (food products during processing), and similar geometries are found in oil drilling operations. We note that if $Re^*_2/Re^*_1 = 0$, then B^* and η^* are related by:

$$B^* = \frac{1}{\eta^* f(\eta^*)}. \tag{6.32}$$

The marginal stability values $Re^*_{1,c}$ are computed as before. These are shown in figure 14(*a*), together with the critical wavenumbers k^*_c, that give maximal growth at critical $Re^*_{1,c}$. For large B^*, the asymptotic behaviour of both $Re^*_{1,c}$ and k^*_c appears to be:

$$Re^*_{1,c} \sim (B^*)^{1.5}, \qquad k^*_c \sim (B^*)^{-0.25}.$$

In terms of the unstarred variables, this is:

$$Re_{1,c} \sim B^{1.25}, \qquad k_c \sim (B)^{0.375}. \tag{6.33}$$

Figure 15 plots the energy estimate stability limits (6.30) and (6.31) against the data from figure 14. We can see that (6.30) and (6.31) are fairly conservative in absolute terms. At fixed η and Re_2/Re_1, (6.31) implies that $k_c Re_{1,c}$ grows at least as fast as $B^{1.5}$ as $B \to \infty$, whereas from our computed data we have $k_c Re_{1,c} \sim B^{1.625}$. Similarly, $Re^*_1 k^* \sim (B^*)^{1.25}$ in our computed results, compared to (6.30). Thus, the actual estimates of the exponents are not overly conservative.

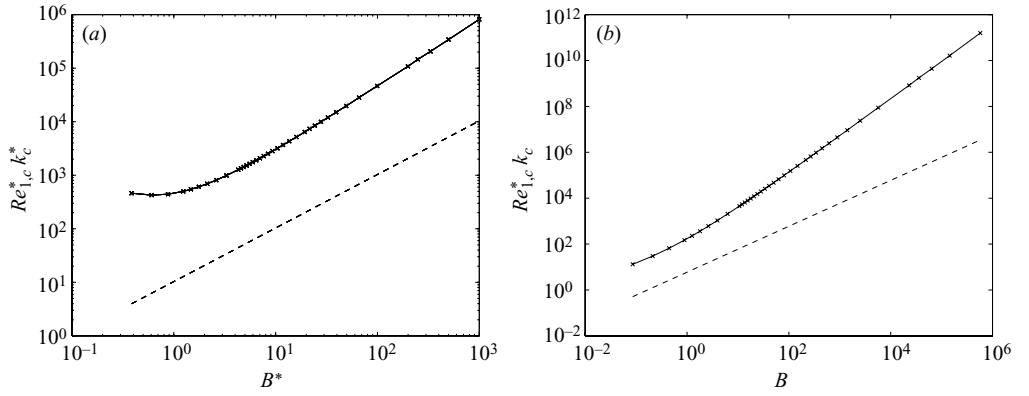

FIGURE 15. Analytic limits for the narrow gap, (6.30) and (6.31), plotted against marginal stability data for the stationary outer cylinder (figure 14): (*a*) $Re_1^* k^*$ *vs.* B^*, dashed line is (6.30); (*b*) $Re_1 k$ *vs.* B^*, dashed line is (6.31).

6.4.1. *Order of magnitude estimate*

We remark that the estimate $Re_{1,c} \sim B^{1.25}$ can also be derived from a simple order of magnitude analysis. Consider the flow between the two cylinders, with stationary outer cylinder in the limit that the yield surface approaches the inner cylinder wall. Suppose that we have a small fluid particle of dimension $\hat{a}$ that is moving radially outwards with speed $\hat{u}_p$. In the absence of any increase in momentum, the particle will decelerate owing to visco-plastic frictional drag from the surrounding fluid. This balance is approximately:

$$\hat{\rho}\hat{a}^3 \frac{\mathrm{d}\hat{u}_p}{\mathrm{d}\hat{t}} \sim -\hat{\mu}_p \hat{u}_p \hat{a} - \hat{\tau}_y \hat{a}^2.$$

Assuming that the yield stress term is dominant, the time scale over which the motion decays is

$$\delta\hat{t} \sim \frac{\hat{\rho}\hat{a}\hat{u}_p}{\hat{\tau}_y},$$

and over this time interval the particle moves a distance $\delta\hat{r} \sim \hat{u}_p \delta\hat{t}$.

In moving a distance $\delta\hat{r}$, the particle may gain momentum from the gradient in the centrifugal force field of the basic flow. This gain is approximately

$$\hat{\rho}\hat{a}^3 \frac{\mathrm{d}}{\mathrm{d}\hat{r}}\left[\frac{\hat{V}^2(\hat{r})}{\hat{r}}\right] \times \delta\hat{r} \sim \frac{\hat{\rho}^2 \hat{u}_p^2 \hat{a}^4 \hat{R}_1 \hat{\Omega}_1^2}{\hat{\tau}_y(\hat{R}_o - \hat{R}_1)},$$

where $\hat{R}_o$ is the dimensional version of R_o, i.e. here is the outer wall of the yielded region. In order for the motion to be sustained, we expect that the gain in momentum from the centrifugal force field gradient at least balances that lost to visco-plastic frictional forces. This balance is captured by:

$$\frac{\hat{\rho}^2 \hat{u}_p^2 \hat{a}^4 \hat{R}_1 \hat{\Omega}_1^2}{\hat{\tau}_y(\hat{R}_o - \hat{R}_1)} \gtrsim \hat{\mu}_p \hat{u}_p \hat{a} + \hat{\tau}_y \hat{a}^2.$$

Dividing throughout by the viscous drag, we have:

$$\frac{\hat{\rho}^2 \hat{u}_p \hat{a}^3 \hat{R}_1 \hat{\Omega}_1^2}{\hat{\tau}_y \hat{\mu}_p(\hat{R}_o - \hat{R}_1)} \gtrsim 1 + \frac{\hat{\tau}_y \hat{a}}{\hat{\mu}_p \hat{u}_p}.$$

The second term on the right-hand side above is effectively a Bingham number, and we consider that this term is much larger than unity as the yield surface approaches the inner cylinder. Neglecting therefore the viscous term, we scale $\hat{a}$ with the yielded gap width $(\hat{R}_o - \hat{R}_1)$ and $\hat{u}_p$ with $\hat{R}_1\hat{\Omega}_1$. After simplifying, this results in the following:

$$\frac{\hat{\rho}^2(\hat{R}_o - \hat{R}_1)^3\hat{R}_1\hat{\Omega}_1^2}{\hat{\mu}_p^2} \gtrsim \left[\frac{\hat{\tau}_y(\hat{R}_o - \hat{R}_1)}{\hat{\mu}_p\hat{R}_1\hat{\Omega}_1}\right]^2.$$

In terms of our dimensionless variables, this balance is exactly:

$$Re_1 \gtrsim B\left[\frac{R_1}{R_o - R_1}\right]^{1/2}.$$

As $B \to \infty$, $(R_o - R_1) \sim B^{-1/2}$, and hence the instability requires $Re_1 \gtrsim B^{1.25}$.

7. Case III solutions and Graebel's narrow gap limit

The second narrow gap limit we can consider is that when Re_2/Re_1 and B remain fixed as $\eta \to 1$. Whereas the narrow gap limit considered above in § 6.3 arises because of an increasing yield stress and consequent growth of the unyielded layer on the outer wall, this limit is purely geometrical. The limit is realized when the radii of the two cylinders become large, whilst maintaining a fixed gap between them. To maintain a Reynolds number ratio $Re_2/Re_1 = 1 - \beta$ implies that $\hat{\Omega}_2/\hat{\Omega}_1 \propto \eta^{-2}(1-\beta)$, whereas maintaining constant B implies that $\hat{\tau}_y/\hat{\mu}_p$ increases as $\hat{R}_1/(\hat{R}_2 - \hat{R}_1) = \eta/(1-\eta) \to \infty$. Considering the plastic viscosity to be fixed, we see that this limit physically implies that $\hat{\tau}_y \to \infty$. However, unlike § 6.3 where $B \to \infty$ can also imply that $\hat{\tau}_y \to \infty$, here we have a distinguished limit. Although our notation is slightly different, this is the same distinguished limit that is evaluated by Graebel (1964). Since there is no physical reason to expect that the yield stress should increase directly proportional to the inner cylinder radius, this narrow gap limit is less applicable than that in § 6.3.

We may see from figure 13(*b*) that $f(\eta) \to 0$ in the limit that $\eta \to 1$, and hence if

$$\frac{Re_2}{Re_1} < 1, \qquad B \text{ fixed}, \tag{7.1}$$

then as $\eta \to 1$, the basic solution for the stability problem will be a case III solution, i.e. yielded across the gap. We therefore restrict our study to case III solutions with $\tau_i < -B/\eta^2$, since it is these that have been found to be unstable. For these we can find τ_i directly and the basic velocity is:

$$V(r) = \frac{Re_2}{Re_1}\left[(1-\eta)r - \frac{\eta^2 r}{1+\eta}\left(\frac{1}{r^2(1-\eta)^2} - 1\right)\right] + \frac{\eta r}{1+\eta}\left(\frac{1}{r^2(1-\eta)^2} - 1\right) + \frac{B\eta^2 r}{1-\eta^2}\left(\frac{1}{r^2(1-\eta)^2} - 1\right)\ln(1/\eta) - Br\ln(1/[r(1-\eta)]). \tag{7.2}$$

Writing $\delta = (1-\eta)$, we find to leading order:

$$\frac{V(r)}{r} \sim \delta\left[\frac{Re_2}{Re_1}\left(\frac{1}{2} + \zeta\right) + \tfrac{1}{2} - \zeta\right] + O(\delta^2), \tag{7.3}$$

$$\frac{\mathrm{d}V}{\mathrm{d}r} \sim \left[\frac{Re_2}{Re_1} - 1\right](1 - \delta\zeta) + 2B\delta\zeta + O(\delta^2), \tag{7.4}$$

$$\left|\frac{\mathrm{d}V}{\mathrm{d}r} - \frac{V(r)}{r}\right| \sim \left[1 - \frac{Re_2}{Re_1}\right] + O(\delta), \tag{7.5}$$

where $\zeta \in [-1/2, 1/2]$ is defined by:

$$r = \frac{1+\eta}{2(1-\eta)} + \zeta.$$

We substitute these expressions into our eigensystem, take the limit as $\delta \to 0$ and retain only the leading-order terms. We have the following leading-order system:

$$\left[1 + \frac{B}{\beta}\right]\left[\mathrm{D}_\zeta^2 - k^2\right]^2 \check{u} - \check{R}e_1(2 - \beta[1+2\zeta])k^2\check{v} = \lambda\left[\mathrm{D}_\zeta^2 - k^2\right]\check{u}, \tag{7.6}$$

$$\left[\mathrm{D}_\zeta^2 - k^2\right]\check{v} - \frac{Bk^2}{\beta}\check{v} + \beta\check{R}e_1\check{u} = \lambda\check{v}, \tag{7.7}$$

where $\mathrm{D}_\zeta = \mathrm{d}/\mathrm{d}\zeta$, where

$$\check{u} = u, \qquad \check{v} = v\delta^{1/2},$$
$$\beta = 1 - \frac{Re_2}{Re_1} > 0, \qquad \check{R}e_1 = \delta^{1/2}Re_1,$$

and where boundary conditions are:

$$\tilde{u} = \mathrm{D}_\zeta\tilde{u} = \tilde{v} = 0 \qquad \text{at} \quad \zeta \pm 1/2. \tag{7.8}$$

Since the effects of large yield stress on stability are represented better by our analysis of case II solutions, we have not invested much effort in solving the above system numerically. The reader may consult Graebel (1964) for an analytical approximation (taking a mean value of the inertial terms), and explicit marginal stability curves. However, there are some differences in notation.

An energy estimate is straightforward to derive. Multiplying (7.6) by $\bar{\check{u}}$, (7.7) by $k^2\bar{\check{v}}$, integrating over $[-1/2, 1/2]$ and summing the real part of the two equations, with liberal use of the Poincaré and Cauchy–Schwarz inequalities, we may derive the estimate:

$$\lambda_R \leqslant \frac{\check{R}e_1[1+\beta/2] - [k^2(1+B/\beta)+\pi^2]}{1 + \dfrac{\|\mathrm{D}_\zeta\check{u}\|^2}{k^2[\|\check{u}\|^2 + \|\check{v}\|^2]}}. \tag{7.9}$$

Therefore, we expect that the flow will be stable in the limit $\eta \to 1$, provided that:

$$Re_1 \leqslant \frac{[k^2(1+B/\beta)+\pi^2]}{(1-\eta)^{1/2}[1+\beta/2]}. \tag{7.10}$$

In this estimate, we note that Re_1 increases with B/β. For sufficiently short wavelengths, B/β essentially just augments the viscosity. This result is in qualitative agreement with Graebel's results.

8. Summary and conclusions

We have presented a range of different results concerning axisymmetric linear perturbations of a Couette flow of a Bingham fluid. Those results presented for counter-rotating cylinders are not surprising, in that they show a steady increase in critical Reynolds number with Bingham number, which confirms the intuitive notion that the yield stress acts to make the fluid behave as if it were simply a more viscous fluid. For co-rotating cylinders this intuition is false, as has been shown independently by Landry (2003) and by Peng & Zhu (2004), i.e. increasing the yield stress can result in a less stable flow.

We have investigated and explained this strange behaviour in § 4.1. There is in fact an $O(1)$ range of B over which $Re_{1,c}$ first decreases and then increases. This effect is more observable for smaller radius ratios. For sufficiently small B, the fluid remains unyielded throughout the annulus. Examination of the linear energy equation has shown that λ_R is destabilized only by the inertial terms, which transfer energy from the basic flow. The basic flow rate of strain $\dot{\gamma}(\boldsymbol{U})$ amplifies the quadratic product of radial and azimuthal velocities in the inertial term. In the co-rotating cylinder regime, we observe that $\dot{\gamma}(\boldsymbol{U})$ in fact increases with B close to the inner cylinder. Conversely, $\dot{\gamma}(\boldsymbol{U})$ divides quadratic products of the perturbation velocities in the yield stress dissipation functional. Thus, for small B we have shown that it is possible for the destabilizing inertial terms to grow with B while the dissipative terms do not. This explains the interesting effect of Landry (2003) and Peng & Zhu (2004).

Eventually, unyielded fluid layers appear at the outer cylinder and move progressively inwards, which results in dominance of the dissipative terms. We have investigated this effect analytically via a narrow gap approximation and shown that $Re_{1,c}k_c \gtrsim B^{1.5}$ as $B \to \infty$. This compares well with our computed results at large B for a stationary outer cylinder: $Re_{1,c} \sim B^{1.25}$ and $k_c \sim B^{0.375}$. We have also shown how $Re_{1,c} \sim B^{1.25}$ can be deduced from a simple order of magnitude analysis, for a stationary outer cylinder.

We have also briefly considered the second (classical) narrow gap limit in which the radius ratio η, approaches unity, for fixed B and Reynolds number ratio. We have shown that $Re_{1,c} \gtrsim (k^2[1 + O(B)] + \pi^2)/(1 - \eta)^{1/2}$ in this limit. Thus, for this limit the principal influence of B is to augment the viscosity, i.e. to stabilize. This limit corresponds to the narrow gap limit considered by Graebel (1964), and we concur with his analysis that B is stabilizing. There is no contradiction with the results of Landry (2003) and Peng & Zhu (2004), since the non-monotonicity of $Re_{1,c}$ is observed for smaller radius ratio cylinders, i.e. away from Graebel's $\eta \to 1$ limit. Furthermore, in comparison with the narrow gap limit in § 6.3, Graebel's distinguished limit $\eta \to 1$ for B fixed is of limited practical use. Graebel's limit implies that the yield stress increases in direct proportion to $\hat{R}_1/(\hat{R}_2 - \hat{R}_1)$, whereas the limit in § 6.3 is purely a large yield stress limit.

An interesting feature of this stability problem is that for the case II base solutions, (which incorporates all solutions as $B \to \infty$), there exists a similarity mapping of both the base solution and stability problem. This mapping of the stability problem, onto an equivalent problem with an outer cylinder of radius exactly equal to the yield surface radius, is possible only because the boundary and compatibility conditions are homogeneous. Such mappings are in fact common for linear stability studies of yield stress fluids (see e.g. Frigaard *et al.* 1994; Frigaard 2001), and result from the linear stability problem being defined only on the yielded region of the flow. Although mathematically equivalent, physically, the transformed problems are not equivalent. In particular, the non-transformed problem does allow a yield surface perturbation. As is common in these problems, the yield surface perturbation decouples from computation of the velocity and pressure perturbations, and plays no role in determining stability.

A natural question, not raised before, is whether or not vortical instabilities will in fact be observable where predicted by the linear analysis. In the case where there is no unyielded fluid, we should expect that vortices can be found. For case II solutions, however, we doubt that the mathematical prediction will be realized in practice. The linear analysis suggests that a vortical structure will grow, bounded on the outside by an unyielded plug region. Whereas robustly stable static unyielded regions can be found bounding outer walls in shear flows (see e.g. Allouche, Frigaard & Sona 2000;

Frigaard, Scherzer & Sona 2001; Frigaard, Leimgruber & Scherzer 2002) here the 'interface stress', between the static region and the yielded region will be at exactly the yield value. As the linear perturbation grows to some saturation amplitude, it is unlikely that the velocity and shear stress perturbations will vanish at exactly the unperturbed yield surface position. Indeed, the vortical structure implies a repeating vertical array of: upwards shear flow, suction, downwards shear flow and impinging jet, all bounding a marginally static yield surface. It is likely that some form of erosion of the plug region will occur, and potentially this can delay transition. This, however, requires further investigation with computational and/or experimental methods.

This work has been partly funded by the BC Advanced Systems Institute and by Metso Corporation. We are grateful for this financial support.

REFERENCES

Allouche, M., Frigaard, I. A. & Sona, G. 2000 Static wall layers in the displacement of two visco-plastic fluids in a plane channel. *J. Fluid Mech.* **424**, 243–277.

Al-Mubaiyedh, U. A., Sureshkumar, R. & Khomami, B. 2000 Linear stability of viscoelastic Taylor–Couette flow: influence of fluid rheology and energetics. *J. Rheol.* **44**, 1121–1138.

Andereck, C. D., Liu, S. S. & Swinney, H. L. 1986 Flow regimes in a circular circular Couette system with independently rotating cylinders. *J. Fluid Mech.* **164**, 155–183.

Avgousti, M. & Beris, A. N. 1993 Non-axisymmetric modes in the viscoelastic Taylor–Couette flow. *J. Non-Newtonian Fluid Mech.* **50**, 225–251.

Bailey, W. J. & Peden, J. M. 2000 A generalized and consistent pressure drop and flow regime transition model for drilling hydraulics. *Soc. Petr. Eng.* paper SPE 62167.

Bingham, E. C. 1922 *Fluidity and Plasticity*, pp. 215–218, McGraw-Hill.

Bird, R. B., Dai, G. C. & Yarusso, B. J. 1983 The rheology and flow of visco-plastic materials. *Rev. Chem. Engng* **1**, 1–70.

Chandrasekhar, S. 1961 *Hydrodynamic and Hydromagnetic Stability*. Dover.

Chossat, P. & Iooss, G. 1994 *The Couette–Taylor Problem*. Springer.

Coronado, O., Souza Mendes, P. F. & Carvalho, M. S. 2002 Taylor–Couette instability of viscoplastic liquids. *74th Society of Rheology Annual Meeting, Minneapolis, Minnesota, October 13–18, 2002.*

Coronado-Matutti, O., Souza Mendes, P. F. & Carvalho, M. S. 2004 Instability of inelastic shear-thinning liquids in a Couette flow between concentric cylinders. *Trans. ASME I: J. Fluids Engng* **126**, 385–390.

Diaz, H., Miska, S., Takach, N. & Yu, M. 2004 Modeling of ECD in casing drilling operations and comparison with experimental and field data. *Soc. Petr. Eng.* paper SPE 87149.

Di Prima, R. C. & Swinney, H. L. 1981 Instabilities and transition in flow between concentric rotating cylinders. In *Hydrodynamic Instabilities and the Transition to Turbulence*. Springer.

Duvaut, G. & Lions, J. L. 1976 *Inequalities in Mechanics and Physics*, pp. 279–327, Springer.

Drazin, P. G. 2002 *Introduction to Hydrodynamic Stability*. Cambridge University Press.

Drazin, P. G. & Reid, W. H. 1981 *Hydrodynamic Stability*. Cambridge University Press.

Fitt, A. D. & Please, C. P. 2001 Asymptotic analysis of the flow of shear-thinning foodstuffs in annular scraped heat exchangers. *J. Engng Maths* **39**, 345–366.

Frigaard, I. A. 2001 Super-stable parallel flows of multiple visco-plastic fluids. *J. Non-Newtonian Fluid Mech.* **100**, 49–76.

Frigaard, I. A., Howison, S. D. & Sobey, I. J. 1994 On the stability of Poiseuille flow of a Bingham Fluid. *J. Fluid Mech.* **263**, 133–150.

Frigaard, I. A., Scherzer, O. & Sona, G. 2001 Uniqueness and non-uniqueness in the steady displacement of two viscoplastic fluids. *Z. Angew. Math. Mech.* **81**, 99–118.

Frigaard, I. A., Leimgruber, S. & Scherzer, O. 2002 Variational methods and maximal residual wall layers. *J. Fluid Mech.* **483**, 37–65.

Graebel, W. P. 1964 The hydrodynamic stability of a Bingham fluid in Couette flow. In *Proceedings of International Symposium on 2nd Order Effects in Elasticity, Plasticity and Fluid Dynamics,*

Haifa, Israel, April 23–27, 1962 (ed. M. Reiner & D. Abir), pp. 636–649. Jerusalem Academic Press.

Hansen, S. A., Rommetveit, R., Sterri, N., Aas, B. & Merlo, A. 1999 A new hydraulics model for slim hole drilling applications. *Soc. Petr. Eng.* paper SPE 57579.

Joo, Y. L. & Shaqfeh, E. S. G. 1992 A purely elastic instability in Dean and Taylor–Dean flow. *Phys. Fluids* A **4**, 524–542.

Joo, Y. L. & Shaqfeh, E. S. G. 1994 Observations of purely elastic instabilities in the Taylor–Dean flow of a Boger fluid. *J. Fluid Mech.* **262**, 27–73.

Khayat, R. E. 1995 Onset of Taylor vortices and chaos in viscoelastic fluids. *Phys. Fluids* **7**, 2191–2219.

Khayat, R. E. 1997 Low-dimensional approach to nonlinear overstability of purely elastic Taylor–vortex flow. *Phys. Rev. Lett.* **78**, 4918–4921.

Khayat, R. E. 1999 Finite-amplitude Taylor-vortex flow of viscoelastic fluids. *J. Fluid Mech.* **400**, 33–58.

Koschmeider, E. L. 1993 *Bénard Cells and Taylor Vortices.* Cambridge University Press.

Landry, M. P. 2003 Taylor–Couette instability of a Bingham Fluid. MSc thesis University of British Columbia.

Larson, R. G. 1989 Taylor–Couette stability analysis for a Doi–Edwards Fluid. *Rheol. Acta* **28**, 504–510.

Larson, R. G. 1992 Instabilities in viscoelastic flows. *Rheol. Acta* **31**, 213–263.

Larson, R. G., Shaqfeh, E. S. G. & Muller, S. J. 1990 A purely elastic instability in Taylor–Couette flow. *J. Fluid Mech.* **218**, 573–600.

Lockett, T. J., Richardson, S. M. & Worraker, W. J. 1992 The stability of inelastic non-Newtonian fluids in Couette flow between concentric cylinders: a finite-element study. *J. Non-Newtonian Fluid Mech.* **43**, 165–177.

Lockett, T. J., Richardson, S. M. & Worraker, W. J. 1993 The importance of rotation effects for efficient cuttings removal during drilling. *Soc. Petr. Eng.* paper SPE 25768.

Loureiro, B. V., Souza Mendes, P. F. & Azevedo, L. F. A. 2006 Taylor–Couette instabilities in tangential annular flow of Newtonain and non-Newtonian liquids in the presence of partial annulus obstruction. *Trans. ASME J. Fluids Engng* **128**, 42–54.

McCann, R. C., Quigley, M. S., Zamora, M. & Slater, K. S. 1993 Effects of high-speed pipe rotation on pressures in narrow annuli. *Soc. Petr. Eng.* paper SPE 26343.

Mossolov, P. P. & Miasnikov, V. P. 1965 Variational methods in the theory of the fluidity of a viscous plastic medium. *J. Mech. Appl. Maths* **29**, 468–492.

Mossolov, P. P. & Miasnikov, V. P. 1966 On stagnant flow regions of a viscous-plastic medium in pipes. *J. Mech. Appl. Maths* **30**, 705–717.

Muller, S. J., Larson, R. G. & Shaqfeh, E. S. G. 1989 A purely elastic transition in Taylor–Couette flow. *Rheol. Acta* **28**, 499–503.

Muller, S. J., Shaqfeh, E. S. G. & Larson, R. G. 1993 Experimental studies of the onset of oscillatory instability in viscoelastic Taylor–Couette flow. *J. Non-Newtonian Fluid Mech.* **46**, 315–330.

Naimi, M., Devienne, R. & Lebouche, M. 1990 Etude dynamique et thermique de l'écoulement de Couette–Taylor–Poiseuille; cas d'un fluide présentant un seuil d'écoulement. *Intl J. Heat. Mass Transfer* **33**, 381–391.

Nouar, C., Devienne, R. & Lebouche, M. 1987 Convection thermique pour l'écoulement de Couette avec debit axial; cas d'un fluide pseudo-plastique. *Intl J. Heat. Mass Transfer* **30**, 639–647.

Nsom, B. & Mangel, H. 2001 Stability of Taylor–Dean flow of Bingham fluid. in proceedings of *International Couette–Taylor Workshop, Evanston, USA, September 6–8, 2001.*

Oldroyd, J. G. 1947 Two-dimensional plastic flow of a Bingham solid. *Proc. Camb. Phil. Soc.* **43**, 383–395.

Peng, J. & Zhu, K.-Q. 2004 Linear stability of Bingham fluids in spiral Couette flow. *J. Fluid Mech.* **512**, 21–45.

Prager, W. 1954 On slow visco-plastic flow. Chap. in *Studies in Mathematics and Mechanics* (volume presented to Richard von Mises). Academic.

Rayleigh, Lord 1916 On the dynamics of revolving fluids. *Proc. R. Soc. Lond.* A **93** (648), 148–154.

Schmid, P. J. & Henningson, D. S. 2001 *Stability and Transition in Shear Flows.* Springer.

Shaqfeh, E. S. G. 1996 Purely clastic instabilities in viscometric flows. *Annu. Rev. Fluid Mech.* **28**, 129–185.

Synge, J. L. 1938 On the stability of a viscous liquid between rotating coaxial cylinders. *Proc. R. Soc. Lon.* A **167** (929), pp. 250–256.

Tagg, R. 1994 The Couette–Taylor problem. *Nonlinear Sci. Today* **4**, 2–25.

Taylor, G. I. 1923 Stability of a viscous liquid contained between two rotating cylinders. *Phil. Trans. R. Soc. Lond.* A **223**, 289–343.

Wang, H., Su, Y., Bai, Y., Gao, Z. & Zhang, F. 2000 A new hydraulics model for slim hole drilling applications. *Soc. Petr. Engrs* paper SPE 59265.